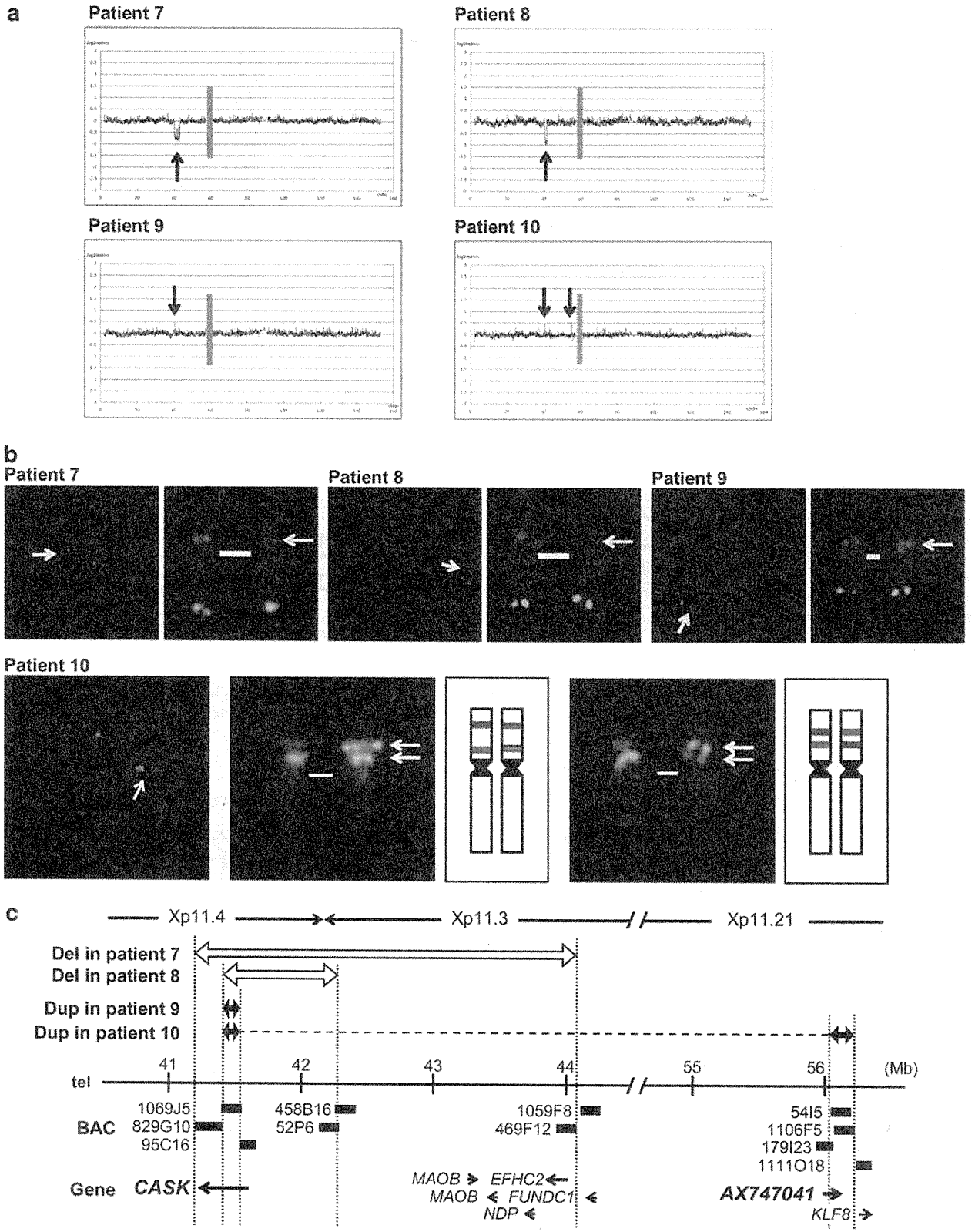
a
Patient 7
Patient 8
Patient 9
Patient 10
b
Patient 7
Patient 8
Patient 9
Patient 10
c
Xp11.4
Xp11.3
Xp11.21
Del in patient 7
Del in patient 8
Dup in patient 9
Dup in patient 10
tel
41
42
43
44
55
56
(Mb)
BAC
1069J5
829G10
95C16
458B16
52P6
1059F8
469F12
54I5
1106F5
179I23
1111O18
Gene
CASK
MAOB
EFHC2
MAOB
FUNDC1
NDP
AX747041
KLF8

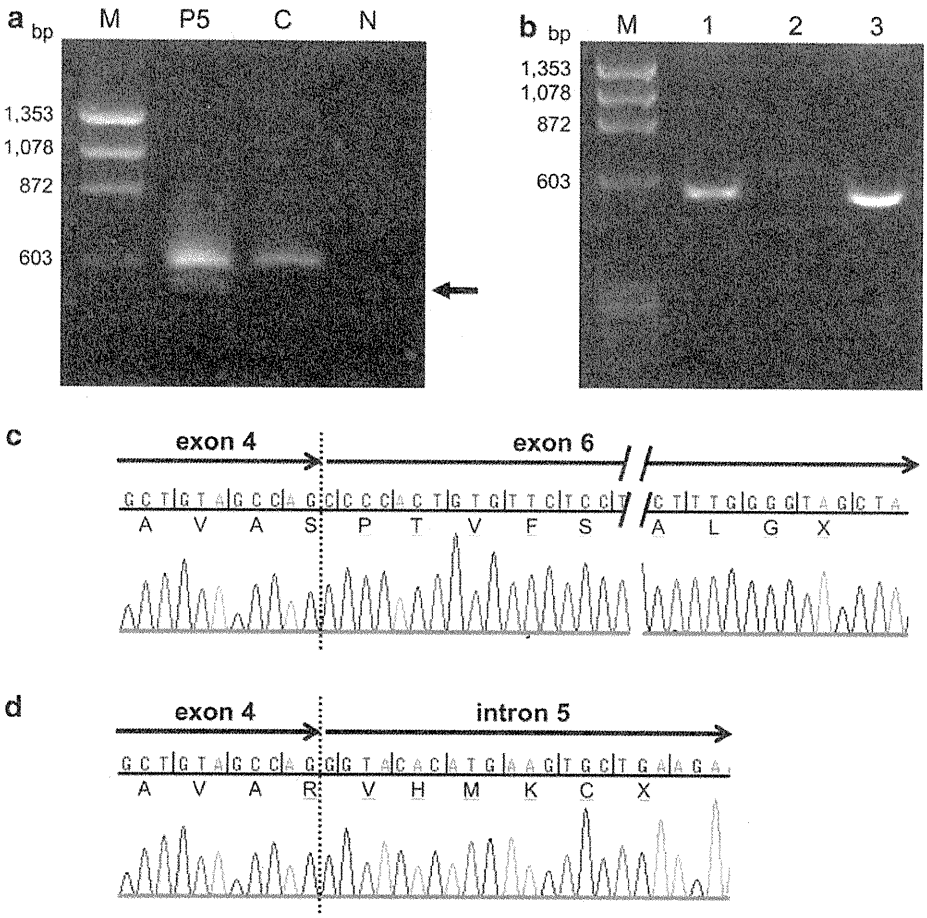

Fig. 4 Exon skipping and aberrant transcripts in patient 5. **a** RT-PCR using primer combinations for exons 3 and 8. The *arrow* indicates an aberrant-sized product in patient 5. *M* marker; ϕX174 RF DNA/Hae III Fragments, *P5* patient 5, *C* control, *N* negative control, no DNA added. **b** The PCR products were cloned to reveal clones of three sizes. Representative clones are shown. No. 1 and no. 3 are aberrant-sized clones and no. 2 is a normal-sized clone. **c**, **d** Sequence chromatograms from clones 1 and 3. In clone 1, exon 5 was skipped to cause an aberrant transcript leading to a frameshift and a premature stop codon in exon 6 (**c**). In clone 3, next to exon 4, exons 5 and 6 were skipped and part of intron 5 was inserted to cause an aberrant transcript leading to a frameshift and a premature stop codon in intron 5 (**d**). The translated amino acid sequences are shown under the nucleotides and *underlines* indicate the frameshift mutations. The *black vertical lines* indicate reading frames. *Dashed vertical lines* denote exon–exon or exon–intron boundaries

et al. 2008) and ours. The molecular mechanism causing the recurrent CNVs remains unclear. For example, known low-copy repeats (LCRs), important factors facilitating nonallelic homologous recombination (NAHR) (Stankiewicz and Lupski 2002), do not adequately explain the CNVs, since no LCRs on/around breakpoints involved in CNVs in any of the current four cases and our previous case (Hayashi et al. 2008) have been registered, even in up-to-date genome databases (UCSC March 2006 and February 2009 build). While the CNVs may be incidental, detailed analyses of the DNA sequence flanking the breakpoints of the CNVs may reveal the mechanisms behind the genomic rearrangement around *CASK* (Inoue et al. 2002).

Recently, *CASK* aberrations have been reported in patients with MR with/without MICPCH (Hsueh 2009) (Table 2). As previously mentioned, a heterozygous nonsense mutation and a disruption caused by a chromosomal inversion were detected in females with severe MR and MICPCH (Najm et al. 2008). They also reported a synonymous mutation causing exon 9 to be skipped in a male, who died at 2 weeks of age. On the other hand, through mutational screening of X-linked MR, four missense mutations of *CASK* were found in male patients with MR (Tarpey et al. 2009). Their MR was mild and two also revealed nystagmus. Moreover, a missense mutation of *CASK* was identified in a family with FG syndrome (Piluso et al., 2009). These reports suggest that *CASK* aberrations cause three very different phenotypes: severe MR with MICPCH in females, mild MR in males and FG syndrome in males, depending on the type of aberration. As *Cask* knockout (KO) mice were reported to die in the neonatal period (Laverty and Wilson 1998; Atasoy et al. 2007), a complete lack of *CASK* is probably lethal, consistent with the male patient with the *CASK* mutation (Najm et al. 2008); however, missense mutations in male patients probably cause different clinical conditions, i.e., mild MR or FG syndrome (Tarpey et al. 2009; Piluso et al. 2009), and haploinsufficiency of

Table 2 Summary of mutations affecting single or few base pairs in the CASK gene

Gender	Phenotype	Type of mutation	Nucleotide change	Protein change	Comment	Report
F	MR/MICPCH	Nonsense	c.1915C>T	*p.R639X*		Najm et al. 2008
M	MR/MICPCH	Synonymous	c.915G > A	*p.=*	Skipping of exon 9 observed; the patient died at 2 weeks	Najm et al. 2008
F	MR/MICPCH	Nonsense	c.79C>T	*p.R27X*		Our case (patient 1)
F	MR/MICPCH	nonsense	c.316C>T	*p.R106X*		Our case (patient 2)
F	MR/MICPCH	Nonsense	c.2632C>T	*p.Q878X*		Our case (patient 3)
F	MR/MICPCH	ins/del	c.243_244delTA	*p.Y81X*		Our case (patient 4)
F	MR/MICPCH	Splice-site mutation	c.357-1G>A	*p.S119Rfs7X* *p.H120Pfs22X*	Skipping of exon 5, or skipping of exon 5 and insertion of partial intron 5	Our case (patient 5)
F	MR/MICPCH	Splice-site mutation	c.2040-1G>C	*p.W680Cfs29X* *p.W680Cfs3X*	Skipping of partial or entire exon 22	Our case (patient 6)
M	FG syndrome	Missense	c.83G>T	*p.R28L*	Skipping of exon 2 observed with low frequency	Piluso et al. 2009
M	Mild MR	Missense	c.2129A>G	*p.D710G*		Tarpey et al. 2009
M	Mild MR	Missense	c.802T>C	*p.Y268H*		Tarpey et al. 2009
M	Mild MR	Missense	c.2767C>T	*p.W914R*		Tarpey et al. 2009
M	Mild MR	Missense	c.1186C>T	*p.P396S*		Tarpey et al. 2009

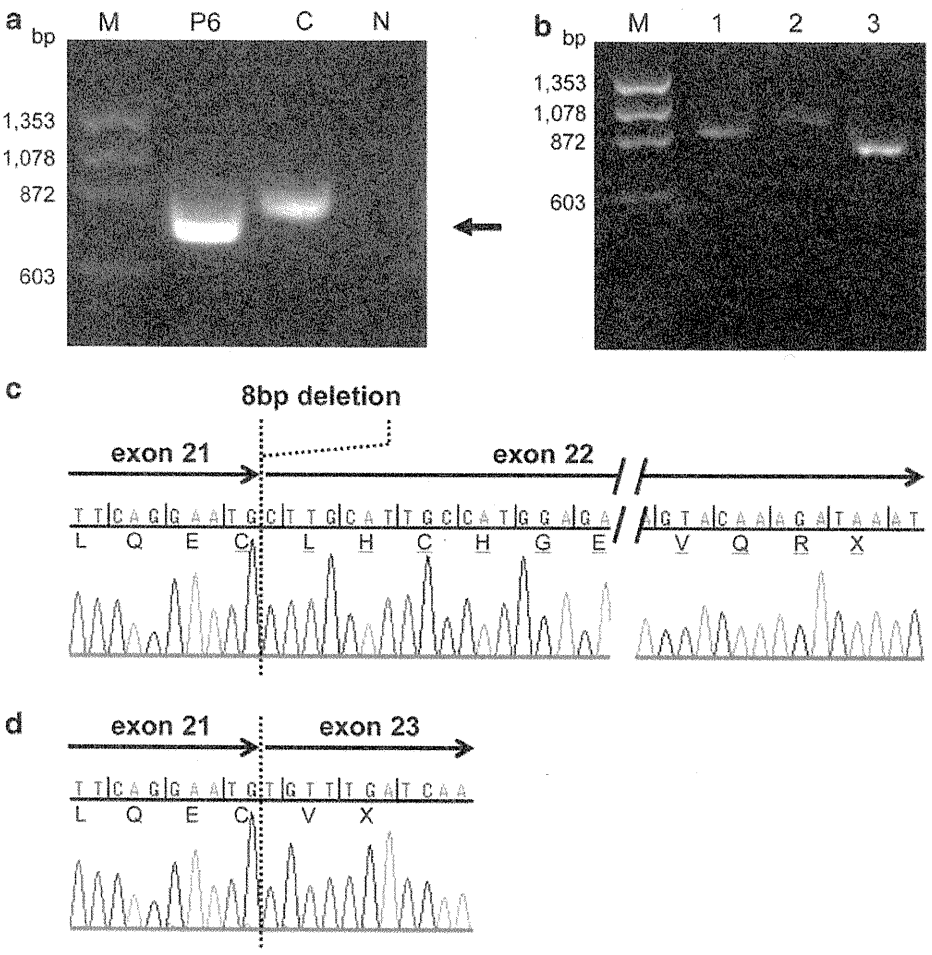

Fig. 5 Exon skipping and aberrant transcripts in patient 6. **a** RT-PCR using primer combinations for exons 19 and 27. The *arrow* indicates an aberrant-sized product in patient 6. *M* marker, ϕX174 RF DNA/Hae III Fragments, *P6* patient 6, *C* control, *N* negative control. **b** The PCR products were cloned to reveal clones of three sizes. Representative clones are shown. No. 1 and 3 are aberrant-sized clones and no. 2 is a normal clone. **c, d.** Sequence chromatograms from clone 1 and 3. In clone 1, the initial 8 bp of exon 22 was absent, causing an aberrant transcript leading to a frameshift and a premature stop codon (**c**). In clone 3, all of exon 22 was missing, resulting in an aberrant transcript leading to a frameshift and a premature stop codon in exon 23 (**d**). The translated amino acid sequences are shown under the nucleotides and *underlines* indicate the frameshift mutations. The *black vertical lines* indicate reading frames. Dashed vertical lines denote exon–exon boundaries

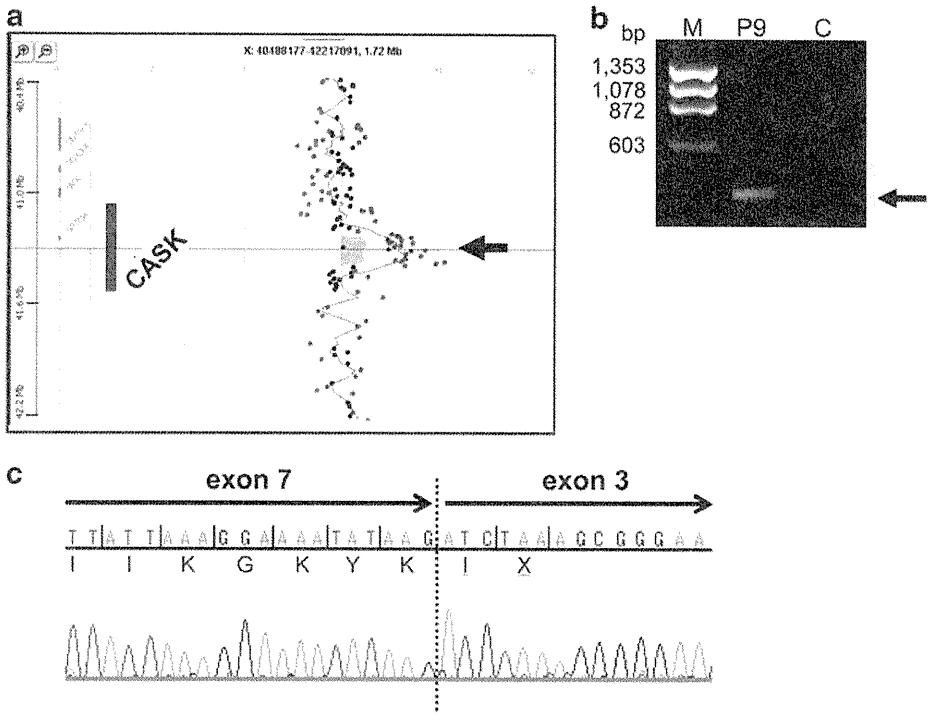

Fig. 6 Analsyses of the duplication in patient 9. **a** Results obtained with Agilent Human Genome CGH microarray kit 244K. This result was described as follows: arr Xp11.4(41,280,790-41,439,415)×3. The duplication included exon 3–7 of *CASK*. It was unclear whether exon 8 was included (*arrow*). The relevant genes are emphasized. **b.** RT-PCR using primer combinations for exon 7 and 4. A product was gained only from patient 9 (*arrow*). *M* marker; ϕX174 RF DNA/Hae III Fragments, *P9* patient 9, *C* control. **c.** Chromatograms for the RT-PCR product shown in (**b**). Next to exon 7, the duplicated exon 3 was transcribed to cause an aberrant transcript leading to a frameshift and a premature stop codon. The translated amino acid sequences are shown under the nucleotides and *underlines* indicate the frameshift mutations. The *black vertical lines* indicate reading frames. *Dashed vertical lines* denote exon–exon boundaries

CASK in females probably causes severe MR with MICPCH (Hayashi et al. 2008; Najm et al. 2008).

CASK encodes a multi-domain scaffolding protein with several critical roles in brain development and synaptic functions, including synaptic interaction, neurotransmitter release and dendritic spine formation (Hata et al. 1996; Irie et al. 1997; Cohen et al. 1998; Hsueh et al. 2000; Olsen et al. 2005; Hsueh 2006; Chao et al. 2008). CASK also regulates the expression of *RELN* involved in brain development through interactions with Tbr-1 via a guanylate kinase (GK)-like domain (Hsueh et al. 2000), and this function may be essential for the etiology of MR with MICPCH. *RELN* plays an important role in neural migration and brain development (D'Arcangelo et al. 1995; Ogawa et al. 1995; Rice et al. 1998), and its mutation is associated with lissencephaly with cerebellar hypoplasia (Hong et al. 2000). While the current analysis provides novel mutations and several types of genomic aberrations of *CASK* causing MR with MICPCH, except for the heterozygous deletions all the mutations and duplications produced aberrant transcripts which will be degraded due to nonsense-mediated mRNA decay and no CASK proteins will be expressed from the mutant alleles; that is, they cause *CASK* null mutations. This may explain the similarity of the phenotypes of MR with MICPCH regardless of the type of *CASK* aberration. The relation between genotypic variety and phenotypic similarity could be clinically useful for detecting and investigating potential patients with *CASK* aberrations.

Web Resources. URLs of the Web sites referred to in this manuscript are as follows:UCSC Genome Bowser, http://genome.ucsc.edu/ (March 2006 build)NCBI, http://www.ncbi.nlm.nih.gov/Online Mendelian Inheritance in Man (OMIM), http://www.ncbi.nlm.nih.gov/Omim/Primer3, http://frodo.wi.mit.edu/primer3/.

Accession Numbers. The *CASK* genomic region is from The UCSC March 2006 build (NCBI36/hg18), range = chrX:41259133-41667231. The GenBank accession number of the human CASK cDNA transcript variant 1 (isoform 1)

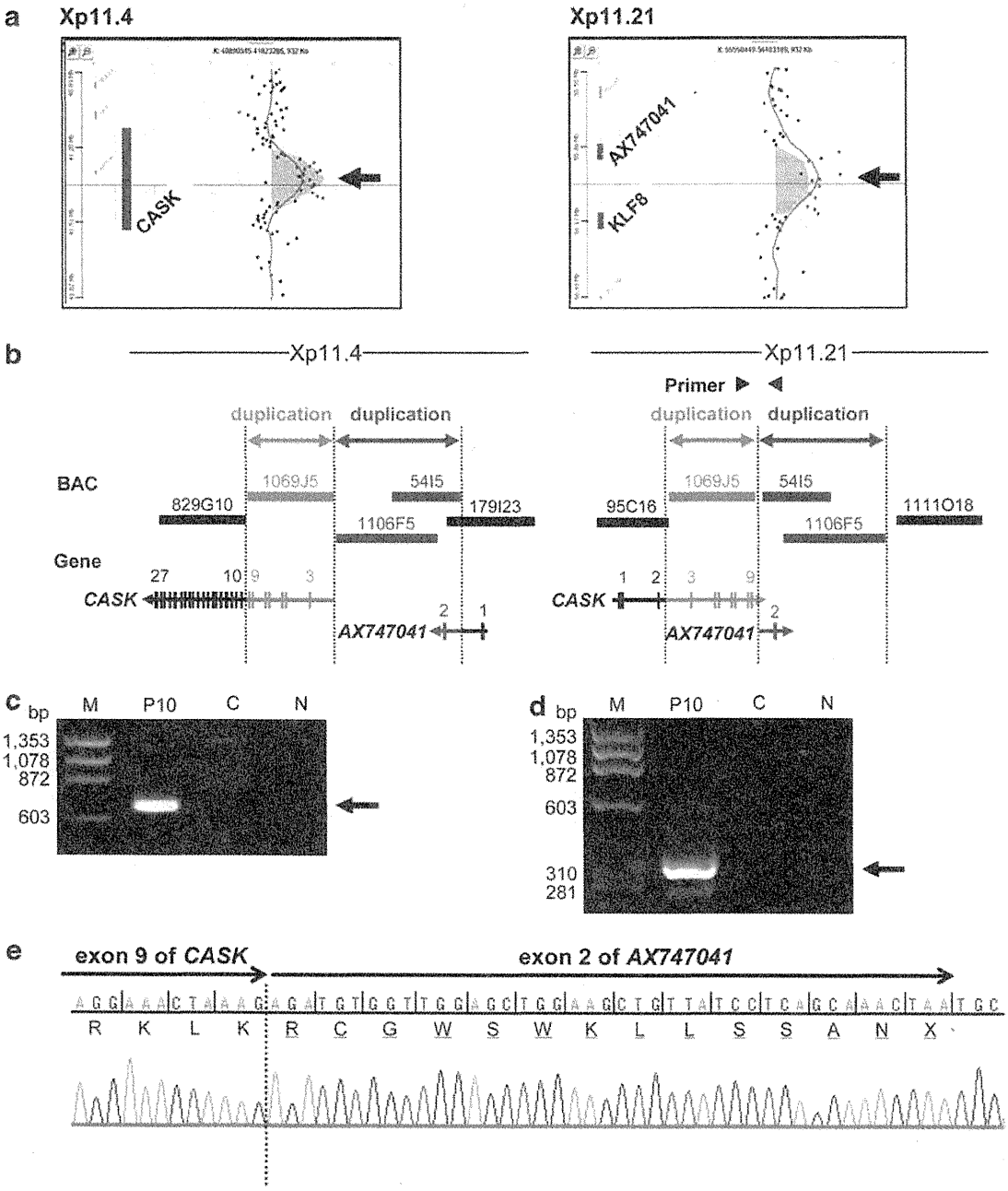

Fig. 7 Analyses of the duplications in patient 10. **a** Results obtained with Agilent Human Genome CGH microarray kit 244K. This result was described as follows: arr Xp11.4(41,381,483-41,539,961)×3, arr Xp11.21(56,022,198-56,272,783)×3. The duplication at Xp11.4 included exons 3–8 of *CASK* (*arrow*, *left panel*) and the duplication at Xp11.21 included exon 2 of *AX747041* (*arrow*, *right panel*). The relevant genes are *emphasized*. **b** A predicted structure of two duplications in patient 10 based on the results of FISH, oligonucleotide array and qPCR. The region denoted by *gray double-headed arrows*, originally at Xp11.4 and including exons 3–9 of *CASK*, was inverted and duplicated at Xp11.21. The region denoted by *red double-headed arrows*, originally at Xp11.21 and including exon 2 of *AX747041*, was inverted and duplicated at Xp11.4. Exons 1 and 2 of CASK and exon 1 of *AX747041* are also involved in the inversion but not duplicated. *Vertical lines* denote exons and *arrows indicate* the direction of *CASK* and *AX747041*, respectively. *Numbers* above the genes denote exons. *Horizontal thick bars* indicate BAC clones (RP-11 series). A pair of *black triangles* indicates the primer combinations for inversion-specific genomic PCR. **c** Inversion-specific PCR revealed a product only in patient 10 (*arrow*). *M* marker; ϕX174 RF DNA/Hae III Fragments, *P10* patient 10, *C* control, *N* negative control. **d** Inversion-specific RT-PCR also revealed a product only in patient 10 (*arrow*). *M* marker; ϕX174 RF DNA/Hae III Fragments, *P10* patient 10, *C* control, *N* negative control. **e** Sequence chromatograms from the RT-PCR product shown in (**d**). Next to exon 9 of *CASK*, exon 2 of *AX747041* was transcribed to cause an aberrant transcript leading to a frameshift and a premature stop codon. The translated amino acid sequences are shown under the nucleotides and *underlines* indicate the frameshift mutations. The *black vertical lines* indicate reading frames. *Dashed vertical lines* denote exon–exon boundaries (color figure online)

and the human CASK protein isoform 1 are NM_003688.3 and NP_003679.2, respectively.

Acknowledgments We thank Ayako Takahashi and Rumi Mori for technical assistance. This study was supported by the Joint Usage/Research Program of Medical Research Institute, Tokyo Medical and Dental University. This work was also supported by Grants-in-Aid for Scientific Research on Priority Areas from the Ministry of Education, Culture, Sports, Science, and Technology, Japan; a grant from Core Research for Evolutional Science and Technology (CREST) of the Japan Science and Technology Corporation (JST); a grant from the New Energy and Industrial Technology Development Organization (NEDO).

References

Atasoy D, Schoch S, Ho A, Nadasy KA, Liu X, Zhang W, Mukherjee K, Nosyreva ED, Fernandez-Chacon R, Missler M, Kavalali ET, Südhof TC (2007) Deletion of CASK in mice is lethal and impairs synaptic function. Proc Natl Acad Sci USA 104:2525–2530

Chao HW, Hong CJ, Huang TN, Lin YL, Hsueh YP (2008) SUMOylation of the MAGUK protein CASK regulates dendritic spinogenesis. J Cell Biol 182:141–155

Cohen AR, Woods DF, Marfatia SM, Walther Z, Chishti AH, Anderson JM (1998) Human CASK/LIN-2 binds syndecan-2 and protein 4.1 and localizes to the basolateral membrane of epithelial cells. J Cell Biol 142:129–138

D'Arcangelo G, Miao GG, Chen SC, Soares HD, Morgan JI, Curran T (1995) A protein related to extracellular matrix proteins deleted in the mouse mutant reeler. Nature 374:719–723

Hata Y, Butz S, Südhof TC (1996) CASK: a novel dlg/PSD95 homolog with an N-terminal calmodulin-dependent protein kinase domain identified by interaction with neurexins. J Neurosci 16:2488–2494

Hayashi S, Kurosawa K, Imoto I, Mizutani S, Inazawa J (2005) Detection of cryptic chromosome aberrations in a patient with a balanced t(1;9)(p34.2;p24) by array-based comparative genomic hybridization. Am J Med Genet A 139:32–36

Hayashi S, Honda S, Minaguchi M, Makita Y, Okamoto N, Kosaki R, Okuyama T, Imoto I, Mizutani S, Inazawa J (2007) Construction of a high-density and high-resolution human chromosome X array for comparative genomic hybridization analysis. J Hum Genet 52:397–405

Hayashi S, Mizuno S, Migita O, Okuyama T, Makita Y, Hata A, Imoto I, Inazawa J (2008) The CASK gene harbored in a deletion detected by array-CGH as a potential candidate for a gene causative of X-linked dominant mental retardation. Am J Med Genet A 146A:2145–2151

Hong SE, Shugart YY, Huang DT, Shahwan SA, Grant PE, Hourihane JO, Martin ND, Walsh CA (2000) Autosomal recessive lissencephaly with cerebellar hypoplasia is associated with RELN mutations. Nat Genet 26:93–96

Hsueh YP (2006) The role of the MAGUK protein CASK in neural development and synaptic function. Curr Med Chem 13:1915–1927

Hsueh YP (2009) Calcium/calmodulin-dependent serine protein kinase and mental retardation. Ann Neurol 66:438–443

Hsueh YP, Wang TF, Yang FC, Sheng M (2000) Nuclear transcription and transcription regulation by the membrane-associated guanylate kinase CASK/LIN-2. Nature 404:298–302

Inazawa J, Inoue J, Imoto I (2004) Comparative genomic hybridization (CGH)-arrays pave the way for identification of novel cancer-related genes. Cancer Sci 95:559–563

Inoue K, Osaka H, Thurston VC, Clarke JT, Yoneyama A, Rosenbarker L, Bird TD, Hodes ME, Shaffer LG, Lupski JR (2002) Genomic rearrangements resulting in PLP1 deletion occur by nonhomologous end joining and cause different dysmyelinating phenotypes in males and females. Am J Hum Genet 71:838–853

Irie M, Hata Y, Takeuchi M, Ichtchenko K, Toyoda A, Hirao K, Takai Y, Rosahl TW, Südhof TC (1997) Binding of neuroligins to PSD-95. Science 277:1511–1515

Laverty HG, Wilson JB (1998) Murine CASK is disrupted in a sex-linked cleft palate mouse mutant. Genomics 53:29–41

Najm J, Horn D, Wimplinger I, Golden JA, Chizhikov VV, Sudi J, Christian SL, Ullmann R, Kuechler A, Haas CA, Flubacher A, Charnas LR, Uyanik G, Frank U, Klopocki E, Dobyns WB, Kutsche K (2008) Mutations of CASK cause an X-linked brain malformation phenotype with microcephaly and hypoplasia of the brainstem and cerebellum. Nat Genet 40:1065–1067

Ogawa M, Miyata T, Nakajima K, Yagyu K, Seike M, Ikenaka K, Yamamoto H, Mikoshiba K (1995) The reeler gene-associated antigen on Cajal-Retzius neurons is a crucial molecule for laminar organization of cortical neurons. Neuron 14:899–912

Olsen O, Moore KA, Fukata M, Kazuta T, Trinidad JC, Kauer FW, Streuli M, Misawa H, Burlingame AL, Nicoll RA, Bredt DS (2005) Neurotransmitter release regulated by a MALS–liprin–alpha presynaptic complex. J Cell Biol 170:1127–1134

Piluso G, D'Amico F, Saccone V, Bismuto E, Rotundo IL, Di Domenico M, Aurino S, Schwartz CE, Neri G, Nigro V (2009) A missense mutation in CASK causes FG syndrome in an Italian family. Am J Hum Genet 84:162–177

Rice DS, Sheldon M, D'Arcangelo G, Nakajima K, Goldowitz D, Curran T (1998) Disabled-1 acts downstream of Reelin in a signaling pathway that controls laminar organization in the mammalian brain. Development 125:3719–3729

Saito-Ohara F, Fukuda Y, Ito M, Agarwala KL, Hayashi M, Matsuo M, Imoto I, Yamakawa K, Nakamura Y, Inazawa J (2002) The Xq22 inversion breakpoint interrupted a novel Ras-like GTPase gene in a patient with Duchenne muscular dystrophy and profound mental retardation. Am J Hum Genet 71:637–645

Shaffer LG, Tommerup N (2005) An International System for Human Cytogenetic Nomenclature (2005). Karger, Basel

Stankiewicz P, Lupski JR (2002) Genome architecture, rearrangements and genomic disorders. Trends Genet 18:74–82

Stevenson D, Laverty HG, Wenwieser S, Douglas M, Wilson JB (2000) Mapping and expression analysis of the human CASK gene. Mammalian Genome 11:934–937

Tarpey PS, Smith R, Pleasance E, Whibley A, Edkins S, Hardy C, O'Meara S, Latimer C, Dicks E, Menzies A, Stephens P, Blow M, Greenman C, Xue Y, Tyler-Smith C, Thompson D, Gray K, Andrews J, Barthorpe S, Buck G, Cole J, Dunmore R, Jones D, Maddison M, Mironenko T, Turner R, Turrell K, Varian J, West S, Widaa S, Wray P, Teague J, Butler A, Jenkinson A, Jia M, Richardson D, Shepherd R, Wooster R, Tejada MI, Martinez F, Carvill G, Goliath R, de Brouwer AP, van Bokhoven H, van Esch H, Chelly J, Raynaud M, Ropers HH, Abidi FE, Srivastava AK, Cox J, Luo Y, Mallya U, Moon J, Parnau J, Mohammed S, Tolmie JL, Shoubridge C, Corbett M, Gardner A, Haan E, Rujirabanjerd S, Shaw M, Vandeleur L, Fullston T, Easton DF, Boyle J, Partington M, Hackett A, Field M, Skinner C, Stevenson RE, Bobrow M, Turner G, Schwartz CE, Gecz J, Raymond FL, Futreal PA, Stratton MR (2009) A systematic, large-scale resequencing screen of X-chromosome coding exons in mental retardation. Nat Genet 41:535–543

ARTICLE IN PRESS
JNS-12108; No of Pages 5
Journal of the Neurological Sciences xxx (2011) xxx–xxx
Contents lists available at SciVerse ScienceDirect
Journal of the Neurological Sciences
journal homepage: www.elsevier.com/locate/jns

Hypoperfusion in caudate nuclei in patients with brain–lung–thyroid syndrome

Mitsugu Uematsu [a,*], Kazuhiro Haginoya [b], Atsuo Kikuchi [a], Tojo Nakayama [a], Yousuke Kakisaka [a], Yurika Numata [a], Tomoko Kobayashi [a], Naomi Hino-Fukuyo [a], Ikuma Fujiwara [a], Shigeo Kure [a]

[a] Department of Pediatrics, Tohoku University School of Medicine, Sendai, Japan
[b] Department of Pediatric Neurology, Takuto Rehabilitation Center for Children, Sendai, Japan

ARTICLE INFO

Article history:
Received 20 August 2011
Received in revised form 11 November 2011
Accepted 15 November 2011
Available online xxxx

Keywords:
Brain–lung–thyroid syndrome
NKX2-1
Array CGH
ECD-SPECT
eZIS

ABSTRACT

Mutations in *NKX2-1* cause neurological, pulmonary, and thyroid hormone impairment. Recently, the disease was named brain–lung–thyroid syndrome. Here, we report three patients with brain–lung–thyroid syndrome. All patients were unable to walk until 24 months of age, and still have a staggering gait, without mental retardation. They have also had choreoathetosis since early infancy. Genetic analysis of *NKX2-1* revealed a novel missense mutation (p.Val205Phe) in two patients who were cousins and their maternal families, and a novel 2.6-Mb deletion including *NKX2-1* on chromosome 14 in the other patient. Congenital hypothyroidism was not detected on neonatal screening in the patient with the missense mutation, and frequent respiratory infections were observed in the patient with the deletion in *NKX2-1*. Oral levodopa did not improve the gait disturbance or involuntary movement. The results of ^{99m}Tc-ECD single-photon emission computed tomography (ECD-SPECT) analyzed using the easy Z-score imaging system showed decreased cerebral blood flow in the bilateral basal ganglia, especially in the caudate nuclei, in all three patients, but no brain magnetic resonance imaging (MRI) abnormalities. These brain nuclear image findings indicate that *NKX2-1* haploinsufficiency causes dysfunction of the basal ganglia, especially the caudate nuclei, resulting in choreoathetosis and gait disturbance in this disease.

1. Introduction

NK2 homeobox 1 (*NKX2-1* or *TITF-1*; MIM #600635), which maps on chromosome 14q13, is a member of the *NK-2* gene family of highly conserved homeodomain-containing transcription factors [1,2]. The gene is expressed in the thyroid, bronchial epithelium, and specific areas of the forebrain during development in the mouse [3–5]. Mice homozygous for the disrupted gene are born dead and lack a thyroid gland, lung parenchyma, and pituitary gland, while heterozygous mice develop normally [4]. An abnormality of the gene in humans was first reported in patients with congenital hypothyroidism [6]. Subsequently, heterozygous point mutations in *NKX2-1* were identified in affected members of a family with benign hereditary chorea [7]. Recently, *NKX2-1* was reported as the gene responsible for brain–lung–thyroid syndrome (MIM #610978), which involves symptoms of neurological impairment, pulmonary disorders, and hypothyroidism [8–13]. Respiratory distress during the neonatal period, recurrent respiratory tract infection, and hypothyroidism are common clinical findings. The neurological impairment is characterized by gait disturbance with delayed first walking and choreoathetosis, in the absence of mental retardation or brain magnetic resonance imaging (MRI) abnormalities [13]. However, some affected individuals have had low-average intelligence, learning problems, psychosis and seizures [14–16].

The pathological mechanism of *NKX2-1* haploinsufficiency has been clarified for the hypothyroidism [17] and pulmonary impairment [18,19], but it is still unclear for the neurological symptoms. Most of the neurological deficits, i.e., the gait disturbance and involuntary movements sometimes accompanied with dystonia, dysarthria, action tremor and saccadic abnormalities [20], reflect dysfunction of the control of movement. Therefore, the basal ganglia were considered to be the most important causal lesion [8,14]. The *NKX2-1* null mouse showed severe morphological changes in the basal ganglia, including absence of the globus pallidus and enlargement of the striatum [4]. *NKX2-1* gene expression has been identified as the origin of the pallidum in the mammalian and avian embryonic archistriatum. These studies indicated that *NKX2*-1 is essential for development of the striatum, especially the pallidum rather than the caudate nuclei [5,21,22].

Brain MRI of patients with brain–lung–thyroid syndrome showed no notable abnormalities, except one case report of reduced size and intensity in the pallidum [8]. Previous brain nuclear imaging studies described various findings regarding the basal ganglia, including reduced blood flow in the striatum and thalamus [23], and hypometabolism in the basal ganglia, more prominent in the caudate nuclei [15].

* Corresponding author at: Department of Pediatrics, Tohoku University School of Medicine, 1-1 Seiryo-machi, Aoba-ku, Sendai 980-8574, Japan. Tel: +81 22 717 7287; fax: +81 22 717 7290.
E-mail address: uematsu@bk9.so-net.ne.jp (M. Uematsu).

0022-510X/$ – see front matter © 2011 Elsevier B.V. All rights reserved.
doi:10.1016/j.jns.2011.11.025

Please cite this article as: Uematsu M, et al, Hypoperfusion in caudate nuclei in patients with brain–lung–thyroid syndrome, J Neurol Sci (2011), doi:10.1016/j.jns.2011.11.025

Here, we report three patients with brain–lung–thyroid syndrome in whom the diagnosis was confirmed by genetic examinations. We performed brain nuclear image analysis to investigate the causal lesion for the neurological symptoms.

2. Method

2.1. Clinical findings

We studied three patients (5, 6, and 7 years old; one male and two females) with gait disturbance who visited Tohoku University Hospital between 2008 and 2009 (Table 1).

Patient 1 was the second female child of healthy non-consanguineous parents (Fig. 1). She was born at term without neonatal respiratory problems. Congenital hypothyroidism was noted on neonatal screening and she has been given thyroxin replacement therapy since then. After the age of 1.6 years, she developed recurrent respiratory infections and was admitted to hospital five times in one year. She had normal mental development, but delayed gross motor development. She could sit alone at the age of 12 months and first walked at 38 months. A staggering gait persists. Her trunk and extremes were mildly hypotonic and continuous choreoathetosis was observed during wakefulness and exacerbated by stress.

Patients 2 and 3 were cousins via their maternal families (Fig. 1). Patient 2 was the third female and Patient 3 was an only male child. Both sets of non-consanguineous parents were healthy fathers and affected mothers with mild involuntary movement and a history of delayed first walking. Both patients were born at term without any perinatal complications. Congenital hypothyroidism was diagnosed in the neonatal period by screening in Patient 2, but at the age of 5 years in Patient 3, despite a neonatal screening test. Unlike Patient 1, they had no severe respiratory infections during infancy. Similar to Patient 1, first walking was observed at 30 months in Patient 2 and at 24 months in Patient 3. They also have persistent gait disturbance and choreoathetosis without mental retardation. The neurological examinations in all three patients did not detect any abnormalities, such as muscle weakness, abnormal deep tendon reflexes, or cerebellar manifestations.

Brain MRI in all three patients showed normal brain size, form, and intensity, including the basal ganglia. Oral levodopa (20 mg/kg/day) was given to all three patients, but no obvious improvement in the neurological symptoms was observed.

2.2. Brain nuclear image analysis

All three patients underwent single photon emission computed tomography (SPECT) to evaluate brain function at Tohoku University Hospital using technetium-99 m ethyl cysteinate dimer (ECD, approximately 12 MBq/kg of body weight) as the radiotracer. Twenty minutes after the injection, SPECT images were acquired using a PRISM IRIX (Shimadzu, Kyoto, Japan), with a low-energy, high-resolution, fan-beam collimator. In total, 120 projection datum points in a 128×128 matrix were obtained in 20 min. Using an ODYSSEY computer (Shimadzu), tomograms two pixels thick (5.8 mm) were reconstructed after a high-frequency cutoff with a Butterworth filter.

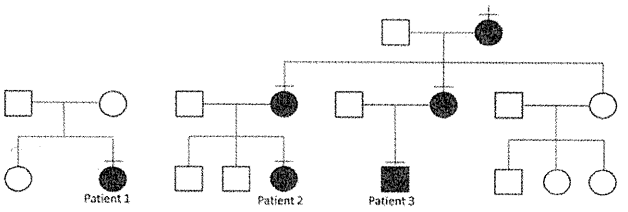

Fig. 1. Family pedigrees of three patients. Affected members are indicated by black squares and circles; unaffected members, white squares and circles. Patient 2 and 3 are cousins on mother's side.

The easy Z-Score Imaging System (eZIS; Fuji Film RI Pharma), used for the statistical analysis of SPECT images, standardizes brain images using Statistical Parametric Mapping (SPM99) [24]. Each SPECT image of the subjects after anatomical standardization followed by isotropic 12-mm smoothing was compared with the mean and SD of SPECT images of the age-matched healthy controls already incorporated in the eZIS program as a normal database using voxel-by-voxel Z-score analysis after voxel normalization to global mean values: Z score = (control mean − individual value)/control SD. These Z-score maps were overlain on tomographic sections and projection with an averaged Z-score of 14-mm thickness to surface rendering of the anatomically standardized MRI template.

Positron emission tomography (PET) was performed in Patients 2 and 3, 1 h after administering [^{18}F]-fluorodeoxyglucose (^{18}FDG) (approximately 3 MBq/kg of body weight) using a Biograph Duo, ECAT EXACT HR^{+} (Siemens, Hoffman Estates, IL) or SET-2400 W (Shimadzu) after fasting for at least 4 h. Emission scans were performed for 10 min for the entire brain. Attenuation was corrected. Fourteen 6-mm-thick slices parallel to the orbitomeatal line, encompassing virtually the entire brain, were analyzed visually by two investigators independently. When the interpretation was inconsistent, a third investigator was called to make a decision.

2.3. Gene analysis

Gene analyses were performed with the informed consent of the patients' parents. Genomic DNA was extracted from peripheral blood lymphocytes using a Sepa Gene kit (Sanko Junyaku, Tokyo, Japan). All coding exons and flanking introns in *NKX2-1* were amplified by PCR. All primers were based on the NCBI reference sequence (accession number NG_013365; the primer sequences are available upon request). The PCR products were separated on 3% agarose gels and purified with a QIAquick Gel Extraction kit (QIAGEN, Chatsworth, CA, USA). The PCR products were sequenced directly using a Big Dye Primer Cycle Sequencing kit and ABI 310 Genetic Analyzer (PE Applied Biosystems, Foster City, CA, USA).

Subsequent array-based comparative genomic hybridization (CGH) analysis was performed using an Agilent 244 K oligonucleotide array (Agilent, Santa Clara, CA; www.agilent.com) with a resolution of approximately 15 kb following the protocols provided by Agilent. The array was analyzed with the Agilent scanner and the Feature Extraction software (v. 9.1.3).

Table 1
Clinical characteristics in three patients.

	Patient 1	Patient 2	Patient 3
Age/sex	7 years/female	5 years/female	6 years/male
Recurrence of respiratory infection	Yes	No	No
Neonatal respiratory problems	No	No	No
Hypothyroidism	Yes (neonatal screening)	Yes (neonatal screening)	Yes (diagnosed at 5 years)
Initiation of walking	3 years and 2 months	2 years and 6 months	2 years
Mental retardation	No	No	No
Choreoathetosis	Yes	Yes	Yes
Response to L-dopa	No	No	No
Brain MRI	Normal	Normal	Normal
NKX2-1 analysis	del 14q12–13	p.V205P	p.V205P

3. Results

From the raw nuclear image ECD-SPECT findings in all three patients (Fig. 2, lower figures) and FDG-PET in Patients 2 and 3

Please cite this article as: Uematsu M, et al, Hypoperfusion in caudate nuclei in patients with brain–lung–thyroid syndrome, J Neurol Sci (2011), doi:10.1016/j.jns.2011.11.025

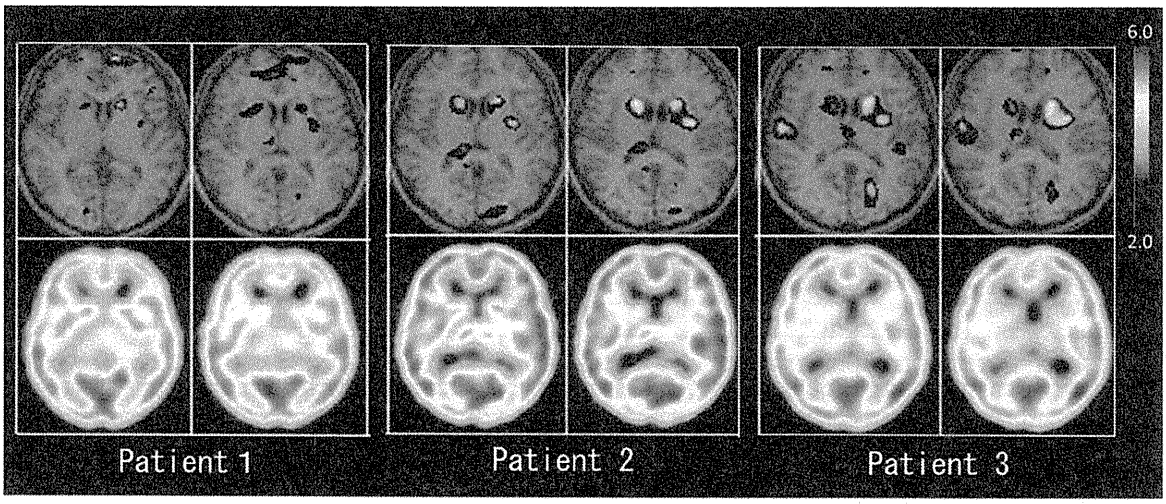

Fig. 2. ECD-SPECT and eZIS results.Usual color images of ECD-SPECT in three patients were shown on the lower figures in each patient. Analyzed images using eZIS were shown on the upper figures. The converted images indicate regions of decreased cerebral blood flow by colors from blue (2.0 standard deviation) to red (6.0 standard deviation). Reduction in cerebral blood flow was shown most common and prominent in the bilateral caudate nuclei in all three patients.

(data not shown), we could not discriminate visible areas of abnormal cerebral perfusion or glucose metabolism. However, the statistical analysis of the ECD-SPECT data using eZIS demonstrated significant declines in cerebral blood flow in the basal ganglia, especially in the caudate nuclei (Fig. 2, upper figure). Although several other brain regions were shown to have decreased blood flow, these were not shared in the three patients.

Array CGH analysis revealed that Patient 1 had an approximately 2.6-Mb hemizygous deletion including *NKX2-1* in 14q12–13 (Fig. 3, top). Direct sequencing analysis revealed a novel hemizygous mutation in the coding exons in Patients 2 and 3 (Fig. 3, bottom), but no mutation in Patient 1. A hemizygous G-to-T substitution at nucleotide position 613 (c.613G>T) in Patients 2 and 3 created an amino acid substitution at amino acid position 205 (p.Val205Phe) within exon 3, which is localized within the *NKX2-1* homeodomain. The mothers and grandmother of Patients 2 and 3 had the same missense mutation.

4. Discussion

In this study, we diagnosed three children with brain–lung–thyroid syndrome based on clinical findings of delayed walking, unsteady gait, choreoathetosis, and hypothyroidism. The diagnosis was confirmed by genetic analysis detecting a novel hemizygous deletion and missense mutations in *NKX2-1*. In addition, we performed nuclear image examinations and analyzed the results using statistical image analysis with eZIS. We found a significant reduction in the blood flow in the caudate nuclei in all three patients.

Recurrent respiratory infection was observed only in the patient with the deletion in *NKX2-1*, but not in the two patients with missense mutations. These phenotype-genotype correlations support previous reports [8,10–13] that large deletions and truncation mutations are related to the severe phenotype with the symptom triad, while missense mutations have a milder phenotype [13]. The existence of respiratory symptoms is very important for management because no deaths have been reported in patients without lung disease [12]. In one case with a missense mutation, hypothyroidism was not detected until the age of 5 years, while it was detected in his cousin with the same mutation at neonatal screening. This interfamilial heterogeneity, as described previously [25], indicates that simple haploinsufficiency cannot fully explain the spectrum of clinical presentations. Other modifying genes might contribute to the phenotype heterogeneity [9,12].

Central nervous impairment is the most common and essential symptom in brain–lung–thyroid syndrome [12,13]. Typically, mental retardation and brain MRI abnormalities are not associated with this disease. The characteristic presentation involves delayed walking, a staggering gait, and choreoathetosis. Since no obvious nervous system abnormalities were detected on neurological examinations, we speculate that the choreoathetosis in the lower limbs caused the delay in walking and unsteady gait.

To identify the brain region responsible for the neurological impairment, we examined brain ECD-SPECT and FDG-PET, but no obvious pathological abnormalities were detected on visual inspection of the raw images. Further statistical analysis of the ECD-SPECT data was performed using eZIS, while the FDG-PET was not analyzed because we did not have an appropriate analysis method. The eZIS method can detect a significant difference of regional cerebral blood flow by comparison with age-matched normal controls, and shows the result as color images. Previous reports described significant superiority of this program over visual inspection of raw SPECT images in several diseases [26–28]. We analyzed our patients and found a common, significant reduction in cerebral blood flow in the caudate nuclei. Although most reports describe expression of the *NKX2-1* gene in the pallidum [8,21,22], a recent study showed *NKX2-1* expression in the postnatal mouse striatum, including the caudate nuclei, in addition to the pallidum [29]. In humans, nuclear image studies indicated a reduction in blood flow [23] and glucose metabolism [15] in the basal ganglia. Hypoperfusion in the caudate nuclei was described in a patient with Huntington's disease [30,31], which usually involves chorea. From these reports and our ECD-SPECT findings using eZIS, we believe that the region responsible for the neurological symptoms in brain–lung–thyroid syndrome, pathologically, is the caudate nuclei. We speculate the possible mechanism that the mutation may impair developmental differentiation and organization of the striatum. Huntington's disease, which also involves the caudate nuclei, partially mimics brain–lung–thyroid syndrome clinically, although the latter is easily differentiated by the history of delayed walking.

In our cases, oral L-dopa [32], a dopamine agonist, and clonazepam failed to improve their neurological impairment. Only a few effective treatment for involuntary movement has been reported [13]. Although some reports described the choreatic movements tend to decrease over time [7,23], the movement disability causes severe trouble with daily life, especially writing difficulty resulting in a leaning impairment in

Please cite this article as: Uematsu M, et al, Hypoperfusion in caudate nuclei in patients with brain–lung–thyroid syndrome, J Neurol Sci (2011), doi:10.1016/j.jns.2011.11.025

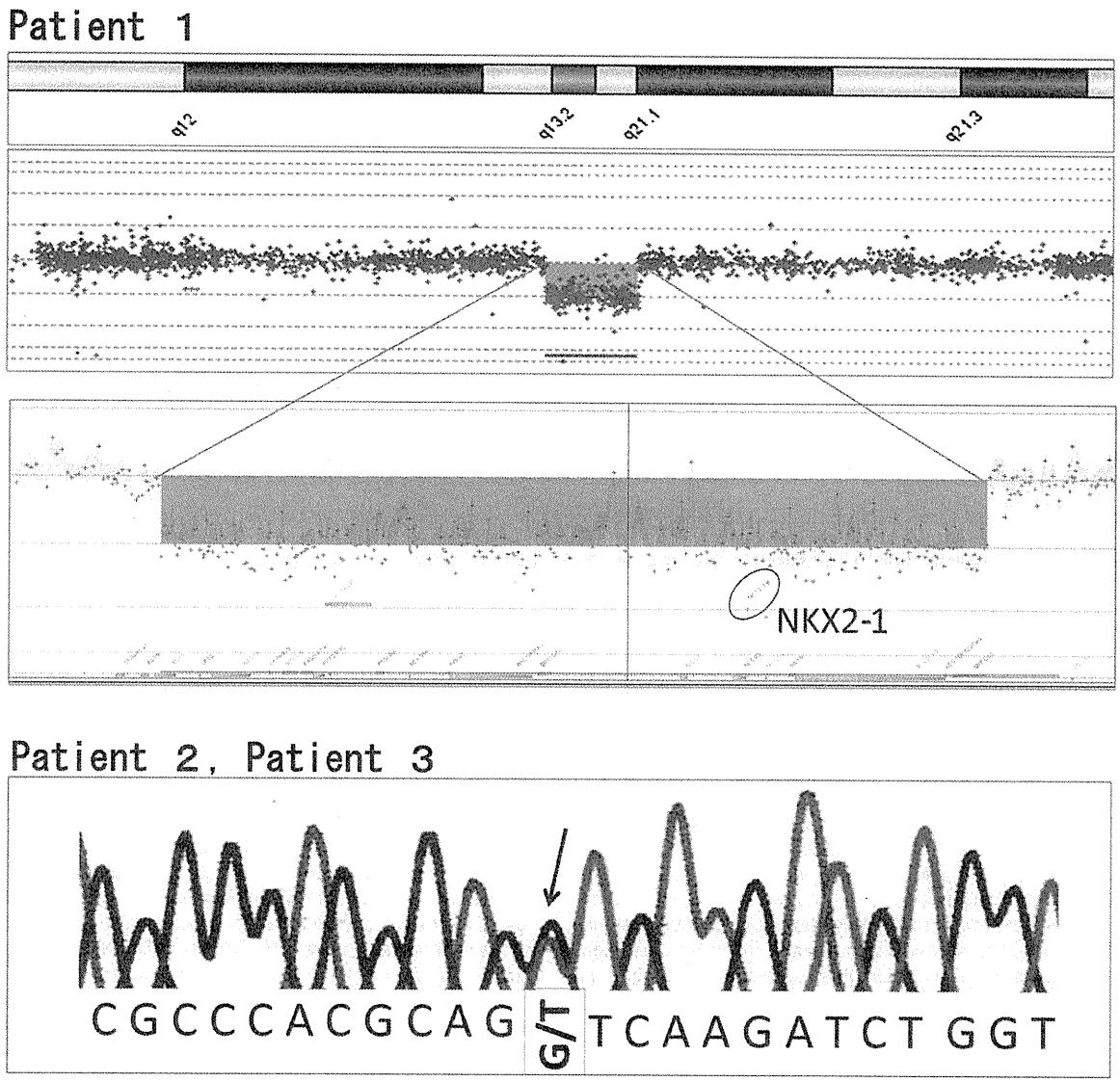

Fig. 3. Deletion and missense mutation in *NKX2-1*. Chromosome 14 profile and detail of 14q12–13 region generated by Cytogenomics (version 1.5, Agilent Technologies) showed a hemizygous 2.6-Mb deletion including *NKX2-1* in Patient 1. Sequencing analysis showed hemizygous missense mutations (c.613G>T) in *NKX2-1* in Patients 2 and 3. (For interpretation of the references to color in this figure legend, the reader is referred to the web version of this article.)

childhood. We postulate that deep brain stimulation might treat involuntary movement, such as in Huntington's disease [33]. The pathophysiology of this disease should be clarified to develop an effective treatment.

Acknowledgments

We are grateful to Ms. Yoko Chiba and Ms. Kumi Itou for their technical assistance.

References

[1] Hamdan H, Liu H, Li C, Jones C, Lee M, deLemos R, et al. Structure of the human Nkx2.1 gene. Biochim Biophys Acta 1998;1396:336–48.
[2] Ikeda K, Clark JC, Shaw-White JR, Stahlman MT, Boutell CJ, Whitsett JA. Gene structure and expression of human thyroid transcription factor-1 in respiratory epithelial cells. J Biol Chem 1995;270:8108–14.
[3] Lazzaro D, Price M, de Felice M, Di Lauro R. The transcription factor TTF-1 is expressed at the onset of thyroid and lung morphogenesis and in restricted regions of the foetal brain. Development 1991;113:1093–104.
[4] Kimura S, Hara Y, Pineau T, Fernandez-Salguero P, Fox CH, Ward JM, et al. The T/ebp null mouse: thyroid-specific enhancer-binding protein is essential for the organogenesis of the thyroid, lung, ventral forebrain, and pituitary. Genes Dev 1996;10:60–9.
[5] Puelles L, Kuwana E, Puelles E, Bulfone A, Shimamura K, Keleher J, et al. Pallial and subpallial derivatives in the embryonic chick and mouse telencephalon, traced by the expression of the genes Dlx-2, Emx-1, Nkx-2.1, Pax-6, and Tbr-1. J Comp Neurol 2000;424:409–38.
[6] Acebron A, Aza-Blanc P, Rossi DL, Lamas L, Santisteban P. Congenital human thyroglobulin defect due to low expression of the thyroid-specific transcription factor TTF-1. J Clin Invest 1995;96:781–5.
[7] Breedveld GJ, van Dongen JW, Danesino C, Guala A, Percy AK, Dure LS, et al. Mutations in TITF-1 are associated with benign hereditary chorea. Hum Mol Genet 2002;11:971–9.
[8] Krude H, Schutz B, Biebermann H, von Moers A, Schnabel D, Neitzel H, et al. Choreoathetosis, hypothyroidism, and pulmonary alterations due to human NKX2-1 haploinsufficiency. J Clin Invest 2002;109:475–80.
[9] Breedveld GJ, Percy AK, MacDonald ME, de Vries BB, Yapijakis C, Dure LS, et al. Clinical and genetic heterogeneity in benign hereditary chorea. Neurology 2002;59:579–84.
[10] Willemsen MA, Breedveld GJ, Wouda S, Otten BJ, Yntema JL, Lammens M, et al. Brain–thyroid–lung syndrome: a patient with a severe multi-system disorder due to a de novo mutation in the thyroid transcription factor 1 gene. Eur J Pediatr 2005;164:28–30.
[11] Kleiner-Fisman G, Lang AE. Benign hereditary chorea revisited: a journey to understanding. Mov Disord 2007;22:2297–305 [quiz 452].
[12] Carre A, Szinnai G, Castanet M, Sura-Trueba S, Tron E, Broutin-L'Hermite I, et al. Five new TTF1/NKX2.1 mutations in brain–lung–thyroid syndrome: rescue by PAX8 synergism in one case. Hum Mol Genet 2009;18:2266–76.

Please cite this article as: Uematsu M, et al, Hypoperfusion in caudate nuclei in patients with brain–lung–thyroid syndrome, J Neurol Sci (2011), doi:10.1016/j.jns.2011.11.025

[13] Inzelberg R, Weinberger M, Gak E. Benign hereditary chorea: an update. Parkinsonism Relat Disord 2011;17:301–7.
[14] Carmo Costa M, Costa C, Silva AP, Evangelista P, Santos L, Ferro A, et al. Nonsense mutation in TITF1 in a Portuguese family with benign hereditary chorea. Neurogenetics 2005;6:209–15.
[15] Salvatore E, Di Maio L, Filla A, Ferrara AM, Rinaldi C, Sacca F, et al. Benign hereditary chorea: clinical and neuroimaging features in an Italian family. Mov Disord 2010;25:1491–6.
[16] Butt SJB, Sousa VH, Fuccillo MV, Hjerling-Leffler J, Miyoshi G, Kimura S, et al. The requirement of Nkx2-1 in the temporal specification of cortical interneuron subtypes. Neuron 2008;59:722–32.
[17] Trueba SS. PAX8, TITF1, and FOXE1 gene expression patterns during human development: new insights into human thyroid development and thyroid dysgenesis-associated malformations. J Clin Endocrinol Metabol 2004;90:455–62.
[18] Maeda Y, Davé V, Whitsett J. Transcriptional control of lung morphogenesis. Physiol Rev 2007;87:219–44.
[19] Guillot L, Carré A, Szinnai G, Castanet M, Tron E, Jaubert F, et al. NKX2-1mutations leading to surfactant protein promoter dysregulation cause interstitial lung disease in "Brain–Lung–Thyroid Syndrome". Hum Mutat 2010;31:E1146–62.
[20] Glik A, Vuillaume I, Devos D, Inzelberg R. Psychosis, short stature in benign hereditary chorea: a novel thyroid transcription factor-1 mutation. Mov Disord 2008;23:1744–7.
[21] Sussel L, Marin O, Kimura S, Rubenstein JL. Loss of Nkx2.1 homeobox gene function results in a ventral to dorsal molecular respecification within the basal telencephalon: evidence for a transformation of the pallidum into the striatum. Development 1999;126:3359–70.
[22] Flandin P, Kimura S, Rubenstein JLR. The progenitor zone of the ventral medial ganglionic eminence requires Nkx2-1 to generate most of the globus pallidus but few neocortical interneurons. J Neurosci 2010;30:2812–23.
[23] Mahajnah M, Inbar D, Steinmetz A, Heutink P, Breedveld GJ, Straussberg R. Benign hereditary chorea: clinical, neuroimaging, and genetic findings. J Child Neurol 2007;22:1231–4.
[24] Kanetaka H, Matsuda H, Asada T, Ohnishi T, Yamashita F, Imabayashi E, et al. Effects of partial volume correction on discrimination between very early Alzheimer's dementia and controls using brain perfusion SPECT. Eur J Nucl Med Mol Imaging 2004;31:975–80.
[25] Montanelli L, Tonacchera M. Genetics and phenomics of hypothyroidism and thyroid dys- and agenesis due to PAX8 and TTF1 mutations. Mol Cell Endocrinol 2010;322:64–71.
[26] Matsuda H, Mizumura S, Nagao T, Ota T, Iizuka T, Nemoto K, et al. Automated discrimination between very early Alzheimer disease and controls using an easy Z-score imaging system for multicenter brain perfusion single-photon emission tomography. AJNR Am J Neuroradiol 2007;28:731–6.
[27] Imamura K, Wada-Isoe K, Kowa H, Tanabe Y, Nakashima K. The effect of donepezil on increased regional cerebral blood flow in the posterior cingulate cortex of a patient with Parkinson's disease dementia. Neurocase 2008;14:271–5.
[28] Sasaki M, Nakagawa E, Sugai K, Shimizu Y, Hattori A, Nonoda Y, et al. Brain perfusion SPECT and EEG findings in children with autism spectrum disorders and medically intractable epilepsy. Brain Dev 2010;32:776–82.
[29] Magno L, Catanzariti V, Nitsch R, Krude H, Naumann T. Ongoing expression of Nkx2.1 in the postnatal mouse forebrain: potential for understanding NKX2.1 haploinsufficiency in humans? Brain Res 2009;1304:164–86.
[30] Hasselbalch SG, Oberg G, Sorensen SA, Andersen AR, Waldemar G, Schmidt JF, et al. Reduced regional cerebral blood flow in Huntington's disease studied by SPECT. J Neurol Neurosurg Psychiatry 1992;55:1018–23.
[31] Reynolds Jr NC, Hellman RS, Tikofsky RS, Prost RW, Mark LP, Elejalde BR, et al. Single photon emission computerized tomography (SPECT) in detecting neurodegeneration in Huntington's disease. Nucl Med Commun 2002;23:13–8.
[32] Asmus F, Horber V, Pohlenz J, Schwabe D, Zimprich A, Munz M, et al. A novel TITF-1 mutation causes benign hereditary chorea with response to levodopa. Neurology 2005;64:1952–4.
[33] Kang GA, Heath S, Rothlind J, Starr PA. Long-term follow-up of pallidal deep brain stimulation in two cases of Huntington's disease. J Neurol Neurosurg Psychiatry 2010;82:272–7.

Please cite this article as: Uematsu M, et al, Hypoperfusion in caudate nuclei in patients with brain–lung–thyroid syndrome, J Neurol Sci (2011), doi:10.1016/j.jns.2011.11.025

HMG Advance Access published December 30, 2011

Human Molecular Genetics, 2011 1–8
doi:10.1093/hmg/ddr585

Mutations in genes encoding the glycine cleavage system predispose to neural tube defects in mice and humans

Ayumi Narisawa[1,2], Shoko Komatsuzaki[1], Atsuo Kikuchi[3], Tetsuya Niihori[1], Yoko Aoki[1], Kazuko Fujiwara[4], Mitsuyo Tanemura[5], Akira Hata[6], Yoichi Suzuki[6], Caroline L. Relton[7], James Grinham[8], Kit-Yi Leung[8], Darren Partridge[8], Alexis Robinson[8], Victoria Stone[8], Peter Gustavsson[9], Philip Stanier[8], Andrew J. Copp[8], Nicholas D.E. Greene[8,*], Teiji Tominaga[2], Yoichi Matsubara[1] and Shigeo Kure[1,3,*]

[1]Department of Medical Genetics, [2]Department of Neurosurgery and [3]Department of Pediatrics, Tohoku University School of Medicine, Sendai, Japan, [4]Institute for Enzyme Research, University of Tokushima, Tokushima, Japan, [5]Tanemura Women's Clinic, Nagoya, Japan, [6]Department of Public Health, Chiba University School of Medicine, Chiba, Japan, [7]Human Nutrition Research Centre, Institute for Ageing and Health, Newcastle University, Newcastle upon Tyne, UK, [8]Institute of Child Health, University College London, London, UK and [9]Department of Molecular Medicine and Surgery, Karolinska Institute, Stockholm, Sweden

Received October 26, 2011; Revised November 25, 2011; Accepted December 6, 2011

Neural tube defects (NTDs), including spina bifida and anencephaly, are common birth defects of the central nervous system. The complex multigenic causation of human NTDs, together with the large number of possible candidate genes, has hampered efforts to delineate their molecular basis. Function of folate one-carbon metabolism (FOCM) has been implicated as a key determinant of susceptibility to NTDs. The glycine cleavage system (GCS) is a multi-enzyme component of mitochondrial folate metabolism, and GCS-encoding genes therefore represent candidates for involvement in NTDs. To investigate this possibility, we sequenced the coding regions of the GCS genes: *AMT*, *GCSH* and *GLDC* in NTD patients and controls. Two unique non-synonymous changes were identified in the *AMT* gene that were absent from controls. We also identified a splice acceptor site mutation and five different non-synonymous variants in *GLDC*, which were found to significantly impair enzymatic activity and represent putative causative mutations. In order to functionally test the requirement for GCS activity in neural tube closure, we generated mice that lack GCS activity, through mutation of *AMT*. Homozygous $Amt^{-/-}$ mice developed NTDs at high frequency. Although these NTDs were not preventable by supplemental folic acid, there was a partial rescue by methionine. Overall, our findings suggest that loss-of-function mutations in GCS genes predispose to NTDs in mice and humans. These data highlight the importance of adequate function of mitochondrial folate metabolism in neural tube closure.

INTRODUCTION

Neural tube defects (NTDs), such as spina bifida and anencephaly, are severe birth defects that result from failure of closure of the neural folds during embryonic development (1). Although NTDs are among the commonest birth defects in humans, the causes are still not well understood. This is most likely due to their complex, multifactorial causation

*To whom correspondence should be addressed at: Neural Development Unit, UCL Institute of Child Health, Guilford Street, London, WC1N 1EH, UK. Email: n.greene@ucl.ac.uk (N.D.E.G.); Department of Pediatrics, Tohoku University School of Medicine, 1-1 Seiryomachi, Aobaku, Sendai 980-8574, Japan. Email: kure@med.tohoku.ac.jp (S.Ku.)

which is thought to involve contributions from both genetic and environmental factors (2–4). The potential complexity of NTD genetics is illustrated by the fact that more than 200 different genes give rise to NTDs when mutated in mice (5,6). Moreover, inheritance patterns in humans suggest a multigenic model in which an affected individual may carry two or more risk alleles, which by themselves may be insufficient to cause NTDs (2).

Folate one-carbon metabolism (FOCM) is strongly implicated as a determinant of susceptibility to NTDs since suboptimal maternal folate status and/or elevated homocysteine are established risk factors, whereas periconceptional maternal folic acid supplementation can reduce the occurrence and recurrence of NTDs (7,8). Nevertheless, the precise mechanism by which folate status influences NTD risk remains elusive (7,9). FOCM comprises a network of enzymatic reactions required for synthesis of purines and thymidylate for DNA synthesis, and methionine, which is required for methylation of biomolecules (Fig. 1A) (9). In addition to the cytosol, FOCM also operates in mitochondria, supplying extra one-carbon units to the cytosolic FOCM as formate (Fig. 1A) (10).

Genes that are functionally related to folate metabolism have been subjected to intensive genetic analysis in relation to NTD causation, principally through association studies (reviewed in 3,4,11). In the most extensively studied gene, *MTHFR*, the c.677C>T SNP is associated with NTDs in some, but not all, populations. However, other FOCM-related genes have largely shown non-significant or only mild associations. Given the apparently complex inheritance of the majority of human NTDs, many association studies have been hampered by limitations on sample size. Moreover, although positive associations have been noted for other genes including *DHFR*, *MTHFD1*, *MTRR* and *TYMS* (12,13), these have not been replicated in all populations, and additional studies are required. The hypothesis that genetically determined abnormalities of folate metabolism may contribute to NTD susceptibility is supported by the observation of defects of thymidylate biosynthesis in a proportion of primary cell lines derived from NTDs (14). However, these defects do not correspond with known polymorphisms in FOCM-related genes. Overall, it appears likely that genetic influences on folate metabolism remain to be identified in many NTDs.

A potential link between mitochondrial FOCM and NTDs was suggested by the finding of an association of increased NTD risk with an intronic polymorphism in *MTHFD1L* (15). Another component of mitochondrial FOCM, the glycine cleavage system (GCS), acts to break down glycine to donate one-carbon units to tetrahydrofolate (THF), generating 5,10-methylenetetrahydrofolate (methylene-THF; Fig. 1B) (16,17). The GCS consists of four enzyme components, each of which is required for the glycine cleavage reaction (18,19). The components—glycine dehydrogenase (decarboxylating) (GLDC; P-protein), aminomethlyltransferase (AMT; T-protein), glycine cleavage system protein H (GCSH; H-protein) and dihydrolipoamide dehydrogenase (DLD; L-protein)—are encoded by distinct genes: *GLDC*, *AMT*, *GCSH* and *DLD*, respectively. The functions of *GLDC*, *AMT* and *GCSH* are specific to the GCS, whereas *DLD* encodes a housekeeping enzyme. GCS components have been found to be abundantly expressed in the neuroepithelium during embryogenesis in the rat (20).

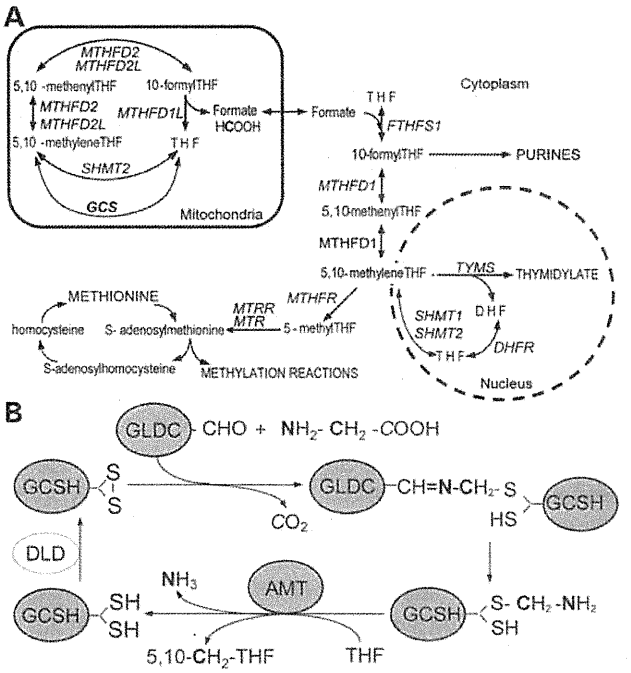

Figure 1. Schematic diagrams summarizing the key reactions of folate-mediated one-carbon metabolism and the GCS. (**A**) Folates donate and accept one-carbon units in the synthesis of purines, thymidylate and methionine. Mitochondrial FOCM supplies one-carbon units to the cytoplasm via formate. The GCS is a key component of mitochondrial FOCM that breaks down glycine and generates 5,10-methylene-THF from THF. Genes encoding enzymes for each reaction are indicated in italics. DHF, dihydrofolate; THF, tetrahydrofolate. (**B**) Summary of the GCS. The glycine cleavage reaction is catalysed by the sequential action of four individual enzymes: GLDC, GCSH, AMT and DLD. The first three of these (shaded grey) are specific to the GCS. Glycine is broken down into CO_2 and NH_3, and donates a one-carbon unit (indicated in bold) to THF, generating 5,10-methylene-THF. The other carbon in glycine (indicated in italics) enters CO_2.

We hypothesized that modulation of GCS activity has the potential to influence efficacy of cellular FOCM during the period of neural tube closure and, hence, susceptibility to NTDs. Therefore, in the current study, we screened genes encoding GCS components for possible mutations in NTD patients and controls. We tested variant proteins for loss of function by enzymatic assay and mice lacking GCS function were generated, to test the effect on embryonic development.

RESULTS

The hypothesis that genes of the GCS represent candidates for involvement in NTDs prompted us to screen for potential mutations in patient samples. Coding exons of *AMT* (9 exons), *GCSH* (5 exons) and *GLDC* (25 exons) were sequenced in a total of 258 NTD patients comprising cohorts from Japan, the UK and Sweden. Each of the major categories of NTDs was represented among study samples, including anencephaly ($n = 38$), spina bifida ($n = 198$) and craniorachischisis ($n = 22$).

Table 1. Nucleotide changes in NTD patients and controls identified by exon sequencing of AMT, GLDC and GCSH

Location	Nucleotide change	Effect	Number of mutation carriers in UK cohorts		Number of mutation carriers in the Japanese cohort		Number of mutation carriers in the Swedish cohort		Variant GLDC enzyme activity[a]
			NTD group (type[b]) ($n = 166$)[c]	Control group ($n = 189$)[c]	NTD group (type[b]) ($n = 14$)[c]	Control group ($n = 36$)[c]	NTD group (type[b]) ($n = 76$)[c]	Control group ($n = 145$)[c]	
AMT									
Exon 2	c.103A>C	p.R35R	0	1	0	0	0	—	
	c.214A>G	p.T72A	0	0	0	1	0	—	
Exon 6	c.623C>A	p.A208D	0	2	0	0	0	—	
	c.631G>A	p.E211K[d]	2 (SBA)	0	0	0	1	—	
	c.589G>C	p.D197H	0	0	1 (An)	0	0	—	
Exon 7	c.825T>A	p.N275K	0	1	0	0	0	—	
	c.850G>C	p.V284L	1 (SBA)	0	0	0	0	—	
GLDC									
Exon 1	c.52G>T	p.G18C	2 (SBO/SBA)	2	0	0	2 (SBA)	2	84%
Exon 5	c.668C>G	p.P223R	0	0	0	1	0	—	92%
Exon 12	c.1508A>C	p.E503A	1 (SBA)	0	0	0	0	0	—
	c.1512G>C	p.E504D	1 (SBA)	0	0	0	0	0	99%
	c.1519G>C	p.G507R	1 (An)	0	0	0	0	0	17%
	c.1525C>G	p.P509A[e]	1 (An)	0	0	0	0	0	41%
	c.1550G>C	p.S517T	0	0	0	0	1 (SBA)	0	—
	c.1570G>C	p.V524L	1 (SBA)	0	0	0	0	0	34%
Exon 14	c.1705G>A	p.A569T[f]	3 (SBA/SBO/SBO)	1	0	0	1 (SBA)	0	40%
Exon 17	c.1953T>C	p.H651H	0	1	0	0	0	—	—
Exon 19	c.2203G>T	p.V735L	0	2	0	0	0	—	81%
Intron 19	c.2316-1G>A	splice	1 (SBA)	0	0	0	0	—	
Exon 20	c.2380G>A	p.A794T	2 (SBASBA)	0	0	0	2 (SBA)	2	88%
	c.2406G>A	p.A802A	1 (An)	0	0	0	0	0	—
Exon 21	c.2474G>A	p.G825D	0	0	1 (An)	0	0	—	24%
	c.2487C>T	p.A829A	0	1	0	0	0	—	—
	c.2565A>C	p.A855A	1 (An)	0	0	0	0	—	—
Exon 23	c.2746C>T	p.L916L	1 (Crn)	0	0	0	0	—	—
Exon 25	c.2964G>A	p.R988R	0	0	0	0	1 (SBA)	0	—
	c.2965A>G	p.I989V	0	1	0	0	0	0	130%
GCSH									
Exon 1	c.53C>T	p.A18V	1 (An)	1	0	0	—	—	

All nucleotide changes were found in heterozygous form. One individual carried c.52G>T and c.1705G>A in *GLDC*, whereas no other individuals carried more than one of the nucleotide changes listed here. Eight silent polymorphisms and four missense variants present in dbSNP (http://www.ncbi.nlm.nih.gov/projects/SNP/) are not listed in this table and include: *AMT*: c.954G>A (p.R318R, rs11715915); *GLDC*: c.249G>A (p.G83G, rs12341698), c.438G>A (p.T146T, rs13289273), c.501G>A (p.E167E, rs13289273), c.660C>T (p.L220L, rs2228095), c.666T>C (p.D222D, rs12004164), c.671G>A (p.R224H, rs28617412) and c.1384C>G (p.L462V, rs73400312); and for *GCSH*: c.62T>C (p.S21L, rs8052579), c.90C>G (p.P30P, rs8177847), c.159C>T (p.F53F, rs177876), c.218A>G (N73S, rs8177876), c.252T>C (Y84Y, rs8177907) and c.261C>G (L87L, rs8177908). Grey shading indicates loss-of-function mutations, based on enzymatic activity in the *in vitro* expression study or splicing defect.

[a]Residual enzymatic activity of GLDC mutant protein is expressed as %activity of the wild-type enzyme (Fig. 2).

[b]SBA, spina bifida aperta; SBO, spina bifida occulta; An, anencephaly; Crn, craniorachischisis.

[c]Total number of UK, Japanese or Swedish NTD patients.

[d]This variant was previously established as likely to be a non-functional polymorphism by segregation in an NKH family (21).

[e]A biochemical test of folate metabolism, the dU suppression test, was previously performed on primary fibroblasts derived from this patient and showed a defect of thymidylate biosynthesis to be present (14).

[f]p.A569T has previously been reported as a pathogenic mutation in a patient with typical NKH (21).

In *AMT*, we identified two novel sequence variants predicted to result in non-synonymous missense changes, c.589G>C (D197H) and c.850G>C (V284L), in anencephaly and spina bifida patients, respectively, from the UK cohort (Table 1). Neither variant was present in 526 UK or 36 Japanese control subjects or in the SNP databases dbSNP and 1000 Genomes. An additional missense variant, E211K, was also identified in three spina bifida patients, two from the UK and one from Sweden. Causative mutations in *AMT* have been found previously in an autosomal recessive inborn error of metabolism, non-ketotic hyperglycaemia (NKH) (17). The E211K variant had previously been identified in an NKH family but was established as likely to be a non-functional polymorphism by segregation (21). Therefore, this variant is considered unlikely to be causally related to NTDs.

Exon sequencing of *GCSH* revealed eight single-base substitutions, one of which (c.53C>T, p.A18V) was a novel change found in both an NTD and a single control (Table 1). The others all corresponded to known SNPs, which did not suggest a role for *GCSH* in NTDs.

Next we turned our attention to *GLDC*, in which we identified 27 single-base substitutions (Table 1), including 11 silent nucleotide changes, 15 non-synonymous changes and a splicing acceptor variant of intron 19 (c.2316-1G>A). The

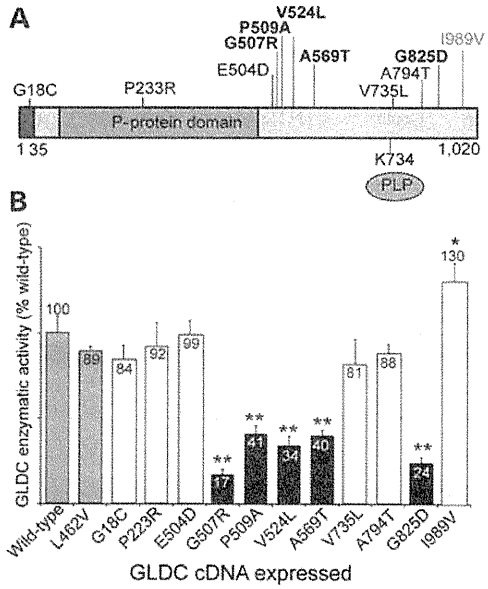

Figure 2. Characterization of *GLDC* missense mutations identified through DNA sequence analysis. (**A**) The schematic represents the 1020 amino acid residue GLDC polypeptide with the positions of the identified missense variants indicated. Mutations conferring significantly reduced activity (**B**) are indicated in bold. The leader peptide for mitochondrial import (shaded black) and the lysine 754-binding site for the co-factor pyridoxal phosphate (PLP) are indicated (49). (B) Enzymatic activity of GLDC missense variants. Expression vectors with wild-type and mutant *GLDC* cDNAs were transfected into COS7 cells for the evaluation of GLDC activity, which is expressed as relative activity (%) of cells expressing wild-type cDNA (shaded grey). The L462V GLDC enzyme (shaded grey) was tested as an example of a normally occurring variant (rs73400312). Variant proteins whose activities were significantly diminished compared with wild-type are indicated by black shading. The I989V variant, identified in a control parent, showed significantly elevated activity. Values are given as mean ± SD of triplicate experiments ($^{*}P < 0.05$; $^{**}P < 0.01$, compared with wild-type).

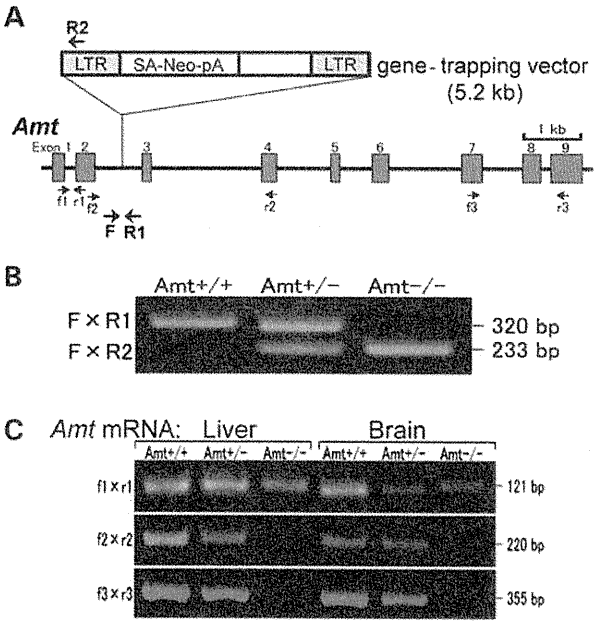

Figure 3. Generation of *Amt* knockout mouse by gene trapping. (**A**) The location of the gene-trap vector in *Amt* intron 2 in the ES cell line OST181110 was determined by inverse PCR. Mice carrying this mutation were generated using standard methods of blastocyst microinjection with OST181110 ES cells to generate chimeras, and germ-line transmission. LTR, long terminal repeats; SA, splicing acceptor site; Neo, neomycin phosphotransferase gene; pA, polyadenylation sequence. (**B**) For genotyping, mouse genomic DNA was subjected to allele-specific amplification with F, R1 and R2 primers (Supplementary Material, Table S1). A genomic fragment of 320 bp was amplified from the wild-type allele, whereas a 233 bp fragment was amplified from the *Amt*-mutant allele. (**C**) RT-PCR analysis of *Amt* mRNA expressed in the brain and liver of *Amt*-mutant mice. Primers in exon 1–2 generated a 121 bp band irrespective of mouse genotypes. RT-PCR in which either one (f2-r2) or both (f3-r3) primers were located in exons 3′ to the insertion site produced 220 and 355 bp cDNA fragments, respectively, in $Amt^{+/+}$ and $Amt^{+/-}$ mice, but not in $Amt^{-/-}$. The *Amt* mRNA in mice carrying the trap vector was, therefore, aberrantly spliced at the end of exon 2, resulting in truncation of *Amt* mRNA in $Amt^{-/-}$ mice.

latter is deduced to abolish normal splicing of the *GLDC* mRNA, with predicted skipping of exon 19 resulting in loss of the reading frame. Among the 15 missense variants identified in *GLDC*, 5 were unique to the NTD group, being absent from all 562 control individuals as well as from the SNP databases. A further three novel variants were found only in controls, whereas the remainder were found in both NTDs and controls, and included previously reported SNPs.

We investigated the possible functional effects of *GLDC* missense variants by expressing wild-type and mutant cDNA constructs in COS7 cells, followed by enzymatic assay of GLDC activity involving a decarboxylation reaction using [1-^{14}C]glycine (22). Twelve GLDC variants were tested, including those that were unique to NTD patients and, therefore, hypothesized to be potentially pathogenic (Fig. 2). The L462V variant, which corresponds to a known SNP (rs73400312), was included as an example of a known normally occurring form. Five of the missense changes, G507R, P509A, V524L, A569T and G825D, resulted in a significant reduction in GLDC activity compared with the wild-type protein ($P < 0.001$). Notably, all five of these deleterious variants were present solely in NTD cases, whereas none of the variants that were unique to controls (P223R, V735L and I989V) showed loss of enzymatic function. In the case of G18C and A794T, which occurred in both NTDs and controls, there was no significant loss of enzymatic activity, suggesting that these are unlikely to be causative mutations.

Having identified putative mutations in *AMT* and *GLDC* in NTD patients, we hypothesized that loss of GCS function could predispose to development of NTDs. In order to directly test the functional requirement for GCS activity in neural tube closure, we generated mice that lacked GCS activity, using a gene trap (OmniBank, OST181110) of the *Amt* gene. The vector was located in intron 2, resulting in a truncated transcript that lacked exons 3–9 (Fig. 3). The efficacy of the gene-trap vector in trapping expression of *Amt* (Amt^{-}) was confirmed by RT-PCR analysis (Fig. 3). Heterozygous $Amt^{+/-}$ mice were viable and fertile and exhibited no obvious malformations. Homozygous $Amt^{-/-}$ mice were not observed among post-natal litters from heterozygote intercrosses, and so fetuses were examined at embryonic day (E) 17.5. Strikingly, 87% of $Amt^{-/-}$ fetuses (34 out of 39) exhibited NTDs, whereas no malformations were observed in $Amt^{+/+}$ ($n = 33$) or $Amt^{+/-}$

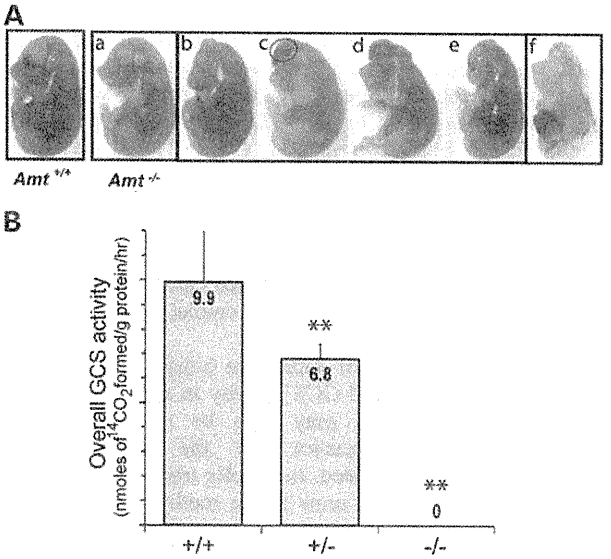

Figure 4. Mice lacking GCS activity exhibit NTDs. (**A**) Phenotypes of *Amt* mutant mice. NTDs were evident in the majority (88%) of $Amt^{-/-}$ fetuses (examples shown are at E17.5). Various types of NTDs were observed in $Amt^{-/-}$ fetuses, which principally affected the cranial region; a, no NTDs; b, small exencephaly (dotted circle); c–e, large exencephaly; f, craniorachischisis. (**B**) Enzymatic activity of the GCS in *Amt* knockout mice. $Amt^{+/-}$ and $Amt^{-/-}$ fetuses had significantly lower GCS activity in the liver than $Amt^{+/+}$ fetuses, with activity in $Amt^{-/-}$ samples below the level of detection ($^{**}P < 0.01$ compared with $Amt^{+/+}$).

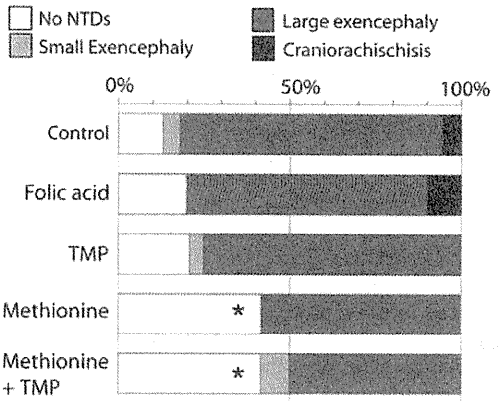

Figure 5. Maternal supplementation of *Amt* mutant embryos with folic acid, TMP or methionine. Maternal treatment with folic acid ($n = 10$ homozygous mutant fetuses) or TMP ($n = 12$) had no significant effect on NTD frequency, whereas the frequency of unaffected embryos was significantly increased following treatment with methionine ($n = 12$) or methionine plus TMP group ($n = 12$). The asterisk indicates significant difference compared with non-treated group ($P < 0.05$).

($n = 66$) fetuses. Defects mainly comprised exencephaly (82%), in which the cranial neural folds persistently failed to close (Fig. 4). There was also a low frequency of the more severe condition, craniorachischisis (5%), in which the neural tube remains open from the mid- and hindbrain, and throughout the spinal region (Fig. 4). Fetal liver samples were subjected to enzyme assay to determine overall activity of the GCS. In $Amt^{-/-}$ mice, overall GCS activity was effectively ablated being below the detection level of the assay (0.01 nmoles of $^{14}CO_2$ formed/gram protein/h), consistent with the Amt^{-} allele being a functional null (22) (Fig. 4). These findings confirm that AMT function is essential for GCS activity, and that the latter is necessary for successful neural tube closure.

Given that GCS is a component of FOCM (Fig. 1), we evaluated the possible prevention of NTDs by folate-related metabolites. Maternal supplementation was performed with folic acid, thymidine monophosphate (TMP), methionine or methionine plus TMP (23). Neither folic acid nor TMP significantly affected the frequency of NTDs among the homozygous $Amt^{-/-}$ offspring. However, we observed a significant protective effect of maternal supplementation with methionine or methionine plus TMP, compared with the non-treated group ($P < 0.05$; Fig. 5).

DISCUSSION

NTDs remain among the commonest human birth defects and understanding their genetic basis presents a considerable challenge owing to their multigenic inheritance and the potential influence of environmental factors, either predisposing or ameliorating. Several lines of evidence indicate a requirement for FOCM in neural tube closure and, therefore, GCS-encoding genes provide excellent candidates for possible involvement in NTD susceptibility. We identified putative mutations in *AMT* and *GLDC* which include a splice acceptor mutation and a number of non-synonymous variants that were absent from a large group of population-matched controls, as well as from public SNP databases. In the case of *GLDC*, enzymatic assay confirmed that several mutations resulted in significant loss of enzyme activity. Finally, *in vivo* functional evidence of a requirement for GCS function in neural tube closure was provided by the occurrence of NTDs in $Amt^{-/-}$ mice lacking GCS activity. Together these findings indicate that mutations in *GLDC* and *AMT* predispose to NTDs in both mice and humans.

Where parental samples were available (6 of the 11 NTD cases that involved putative mutations in *GLDC*), we demonstrated parent-to-child transmission (Supplementary Material, Table S2). Six were instances of maternal transmission and one involved paternal transmission. We hypothesize that absence of an overt NTD phenotype in parents who carry a deficient *GLDC* allele may result from incomplete penetrance, or lack of additional genetic or environmental factors which are predicted to be necessary for NTDs owing to their multifactorial aetiology. We also note that partial penetrance is a feature of numerous mouse models of NTDs (5,8).

Inherited GCS deficiency, owing to mutation of *AMT* and/or *GLDC*, has been shown to cause NKH in humans (17). NKH is a rare, autosomal recessive, inborn error of metabolism, characterized by accumulation of glycine and encephalopathy-like neurological signs, including coma and convulsive seizures in neonates. GCS activity is greatly diminished in NKH patients and they would, therefore, be predicted to be at increased risk of NTDs. It is possible that NTDs may occur in combination with NKH but as anencephaly is a lethal condition, co-existing

NKH would go undetected. Lack of NTDs in NKH patients may also reflect the multigenic nature of NTDs, which require the presence of additional risk alleles in non-GCS genes. NKH is a relatively rare condition, with a prevalence of 1/63 000 births in British Columbia (24) and 1/250 000 in the USA (25). It is therefore possible that an increased risk of NTDs among carriers of GCS mutations in NKH families may not have been noted and this possibility is worthy of investigation. Based on estimated carrier frequency and the incidence of mutations among NTD patients, we predict that NTDs might be expected among 1/150 of the siblings of NKH patients (see Supplementary Material, Table S3 for estimate calculation). One case report of an NKH patient with a *GLDC* mutation describes the additional presence of spinal cord hydromyelia (19). This condition is often associated with low spinal defects (involving secondary neurulation), but it is also possible that the expanded spinal canal was also present at a higher level and might indicate a limited defect in primary neurulation.

The mutations described in the current study were all present in heterozygous form and, therefore, are hypothesized to be insufficient to cause NKH while predisposing to NTDs. For example, in the current study we found four NTD patients and one control individual to be heterozygous for the A569T mutation, which is shown to result in reduced enzyme activity. This mutation was previously identified in a Caucasian patient with typical NKH, in combination with a second mutation, P765S (26), confirming that it is deleterious *in vivo*. Hence, we predict that, depending on the co-existing genetic milieu, the A569T variant may cause NKH, predispose to NTDs or be compatible with normal development.

The high incidence of NTDs in *AMT* mutant mice is particularly notable as NTDs have not previously been found to be a common feature of mouse models deficient for folate-metabolizing enzymes. This includes null mutants that have been reported for eight other genes that encode enzymes in FOCM (Fig. 1A) (27). Four have normal morphology at birth (*Cbs*, *Mthfd1*, *Mthfr* and *Shmt1*) (28–31), *Mthfd2* null embryos die by E15.5 but neural tube closure is complete (32) and null mutants for *Mtr*, *Mtrr* and *Mthfs* die before E9.5, prior to neural tube closure (33–35). Although analysis of mouse mutants has not supported a role for single-gene mutations in FOCM as major causes of NTDs, a requirement for cellular uptake of folate for neural tube closure has been demonstrated in *Folr1* null embryos, in which NTDs occur when rescued from early lethality by folic acid supplementation (36). There is also considerable evidence for possible involvement of gene–environment and/or gene–gene interactions in NTDs. For example, in *Pax3* mutant (*splotch*) embryos, which exhibit a defect of thymidylate biosynthesis, dietary folate-deficiency increases the frequency of cranial NTDs (23,37). Similarly, a diet deficient in folate and choline causes NTDs in *Shmt1* mutant embryos, whereas *Shmt1* and *Pax3* mutations exhibit genetic interaction (38).

Regarding the mechanisms by which GCS mutations affect neural tube closure, a key question is whether NTDs are caused by impairment of FOCM or by another cause such as glycine accumulation. Modelling of hepatic FOCM, based on biochemical properties of folate-metabolizing enzymes (39), predicts that loss of the mitochondrial GCS reaction would reduce the efflux rate of formate to the cytosol by ~50%. This results in reduced synthesis of purines and thymidylate, which are essential for the rapid cell division in the closing neural folds. Interestingly, a UK patient with anencephaly who was found to carry the *GLDC* loss-of-function mutation P509A in the current study (Table 1) was previously found to have impaired thymidylate biosynthesis, assayed in cultured fibroblasts (14). These findings support the hypothetical link between diminished GLDC function, reduced thymidylate biosynthesis and development of NTDs. Reduced thymidylate biosynthesis and diminished cellular proliferation are proposed to underlie folate-related cranial NTDs in *splotch* (*Pax3*) mouse mutants (37,38).

As well as impairment of nucleotide biosynthesis, the predicted effect of diminished GCS activity in reducing production of methionine (39) may also be of relevance as methionine is the precursor for the methyl donor *S*-adenosylmethionine. Indeed, metabolic tracing experiments suggest that ~80% of 1C units in the methylation cycle are generated within mitochondrial FOCM (40). Impairment of the methylation cycle and/or DNA methylation is known to cause NTDs in mice (41) and is proposed as a possible cause of human NTDs (7,42). It was therefore notable that we found a preventive effect of methionine supplementation in $Amt^{-/-}$ mice. Together, these findings suggest that FOCM, required for both thymidylate biosynthesis and methylation reactions that are essential for neural tube closure, may be functionally deficient in individuals who have mutations in *GLDC* or *AMT*.

MATERIALS AND METHODS

Patient cohorts and sequencing

Mutation analysis by DNA sequencing was performed on all exons of *AMT*, *GCSH* and *GLDC* as described (26). Cases comprised Japanese patients with anencephaly ($n = 14$) and two separate cohorts of UK patients with a diagnosis of anencephaly (combined $n = 24$), spina bifida ($n = 122$) or craniorachischisis ($n = 22$). In addition, the exons of *AMT*, *GCSH* and *GLDC* were sequenced in 76 Swedish patients with spina bifida. Unaffected controls, completely sequenced for these genes, comprised 36 Japanese and 189 unrelated UK subjects. Exons found to contain missense mutations were also sequenced in a further cohort of 192 well-characterized UK controls (43) and in 145 Swedish controls. This study was approved by the Ethical Committees of Tohoku University School of Medicine, UCL Institute of Child Health, Newcastle University and the Karolinska Institute.

Enzymatic assay of GCS activity and GLDC activity

GCS activity was measured in mouse liver samples by a decarboxylation reaction using [1-^{14}C]glycine as described (22). For analysis of GLDC activity, wild-type and mutant *GLDC* cDNAs were cloned into pCAG expression vector, kindly provided by Professor Jun-ichi Miyazaki (Osaka University, Japan) (44). Constructs were transfected into COS7 cells, which were harvested as described previously and cell pellets stored at −80°C prior to analysis (45). GLDC

enzymatic activity was determined, in triplicate, by exchange reaction between carbon dioxide and glycine using $NaH^{14}CO_3$ in the presence of excess recombinant bovine GCSH protein as described (22). An expression system of lipoylated bovine GCSH protein in *Escherichia coli* was kindly provided by Dr Kazuko Fujiwara (Tokushima University, Japan) (46). Statistical analysis was performed using SPSS software version 11.0 (SPSS, Inc., Chicago, IL, USA).

Knockout of Amt by insertion of a gene-trap vector

Mice carrying a gene-trap allele of *Amt* (here denoted Amt^{-}) were generated at Lexicon Genetics, Inc. (Houston, TX, USA) using the OST181110 ES cell line. The genomic insertion site of the gene-trap vector was determined by inverse PCR and localized to intron 2 (Supplementary Material, Fig. S1). Total RNA was prepared from the mouse liver and brain at E18 for RT-PCR analysis (Supplementary Material, Fig. S1 and Table S1). $Amt^{+/-}$ mice were backcrossed with wild-type C57BL/6 mice for nine generations to generate a congenic line of mice on the C57BL/6 background, for use in biochemical and histological analyses. This study was approved by the Animal Experiment Committee of Tohoku University.

Maternal supplementation with folic acid and related metabolites

Dams were treated with folic acid (25 mg/kg), thymidine-1-phosphate (TMP; 30 mg/kg) or L-methionine (70 mg/kg) by intra-peritoneal injection, 2 h prior to mating and daily from E7.5–10.5. Doses were based on previous studies (23,47,48).

SUPPLEMENTARY MATERIAL

Supplementary Material is available at *HMG* online.

Conflict of Interest statement. None declared.

FUNDING

This work was supported by a research grant from the Ministry of Education, Culture, Sports, Science and Technology and a Research Grant from the Ministry of Health, Labour and Public Welfare in Japan. Research at Newcastle University was funded by the Newlife Foundation. Research at UCL Institute of Child Health was supported by SPARKS, the Wellcome Trust, Medical Research Council, UCL Biomedical Research Centre and by Great Ormond Street Hospital Children's Charity. Funding to pay the Open Access publication charges for this article was provided by Wellcome Trust.

REFERENCES

1. Greene, N.D. and Copp, A.J. (2009) Development of the vertebrate central nervous system: formation of the neural tube. *Prenatal Diag.*, **29**, 303–311.
2. Harris, M.J. and Juriloff, D.M. (2007) Mouse mutants with neural tube closure defects and their role in understanding human neural tube defects. *Birth Defects Res. A Clin. Mol. Teratol.*, **79**, 187–210.
3. Greene, N.D.E., Stanier, P. and Copp, A.J. (2009) Genetics of human neural tube defects. *Hum. Mol. Genet.*, **18**, R113–R129.
4. Au, K.S., Ashley-Koch, A. and Northrup, H. (2010) Epidemiologic and genetic aspects of spina bifida and other neural tube defects. *Dev. Disabil. Res. Rev.*, **16**, 6–15.
5. Harris, M.J. and Juriloff, D.M. (2010) An update to the list of mouse mutants with neural tube closure defects and advances toward a complete genetic perspective of neural tube closure. *Birth Defects Res. A Clin. Mol. Teratol.*, **88**, 653–669.
6. Copp, A.J. and Greene, N.D.E. (2010) Genetics and development of neural tube defects. *J. Pathol.*, **220**, 217–230.
7. Blom, H.J., Shaw, G.M., Den Heijer, M. and Finnell, R.H. (2006) Neural tube defects and folate: case far from closed. *Nat. Rev. Neurosci.*, **7**, 724–731.
8. Molloy, A.M., Brody, L.C., Mills, J.L., Scott, J.M. and Kirke, P.N. (2009) The search for genetic polymorphisms in the homocysteine/folate pathway that contribute to the etiology of human neural tube defects. *Birth Defects Res. A Clin. Mol. Teratol.*, **85**, 285–294.
9. Beaudin, A.E. and Stover, P.J. (2009) Insights into metabolic mechanisms underlying folate-responsive neural tube defects: a mini review. *Birth Defects Res. A Clin. Mol. Teratol.*, **85**, 274–284.
10. Tibbetts, A.S. and Appling, D.R. (2010) Compartmentalization of mammalian folate-mediated one-carbon metabolism. *Annu. Rev. Nutr.*, **30**, 57–81.
11. Boyles, A.L., Hammock, P. and Speer, M.C. (2005) Candidate gene analysis in human neural tube defects. *Am. J. Med. Genet. C Semin. Med. Genet.*, **135**, 9–23.
12. Shaw, G.M., Lu, W., Zhu, H., Yang, W., Briggs, F.B., Carmichael, S.L., Barcellos, L.F., Lammer, E.J. and Finnell, R.H. (2009) 118 SNPs of folate-related genes and risks of spina bifida and conotruncal heart defects. *BMC Med. Genet.*, **10**, 49.
13. Martinez, C.A., Northrup, H., Lin, J.I., Morrison, A.C., Fletcher, J.M., Tyerman, G.H. and Au, K.S. (2009) Genetic association study of putative functional single nucleotide polymorphisms of genes in folate metabolism and spina bifida. *Am. J. Obstet. Gynecol.*, **201**, 394–411.
14. Dunlevy, L.P.E., Chitty, L.S., Doudney, K., Burren, K.A., Stojilkovic-Mikic, T., Stanier, P., Scott, R., Copp, A.J. and Greene, N.D.E. (2007) Abnormal folate metabolism in foetuses affected by neural tube defects. *Brain*, **130**, 1043–1049.
15. Parle-McDermott, A., Pangilinan, F., O'Brien, K.K., Mills, J.L., Magee, A.M., Troendle, J., Sutton, M., Scott, J.M., Kirke, P.N., Molloy, A.M. and Brody, L.C. (2009) A common variant in MTHFD1L is associated with neural tube defects and mRNA splicing efficiency. *Hum. Mutat.*, **30**, 1650–1656.
16. Kikuchi, G. (1973) The glycine cleavage system: composition, reaction mechanism, and physiological significance. *Mol. Cell. Biochem.*, **1**, 169–187.
17. Kure, S., Tada, K. and Narisawa, K. (1997) Nonketotic hyperglycinemia: biochemical, molecular, and neurological aspects. *Jpn J. Hum. Genet*, **42**, 13–22.
18. Kure, S., Narisawa, K. and Tada, K. (1992) Enzymatic diagnosis of nonketotic hyperglycinemia with lymphoblasts. *J. Pediatr.*, **120**, 95–98.
19. Hayasaka, K., Tada, K., Kikuchi, G., Winter, S. and Nyhan, W.L. (1983) Nonketotic hyperglycinemia: two patients with primary defects of P-protein and T-protein, respectively, in the glycine cleavage system. *Pediatr. Res.*, **17**, 967–970.
20. Ichinohe, A., Kure, S., Mikawa, S., Ueki, T., Kojima, K., Fujiwara, K., Iinuma, K., Matsubara, Y. and Sato, K. (2004) Glycine cleavage system in neurogenic regions. *Eur. J. Neurosci.*, **19**, 2365–2370.
21. Toone, J.R., Applegarth, D.A., Kure, S., Coulter-Mackie, M.B., Sazegar, P., Kojima, K. and Ichinohe, A. (2002) Novel mutations in the P-protein (glycine decarboxylase) gene in patients with glycine encephalopathy (non-ketotic hyperglycinemia). *Mol. Genet. Metab.*, **76**, 243–249.
22. Sakata, Y., Owada, Y., Sato, K., Kojima, K., Hisanaga, K., Shinka, T., Suzuki, Y., Aoki, Y., Satoh, J., Kondo, H. *et al.* (2001) Structure and expression of the glycine cleavage system in rat central nervous system. *Brain Res. Mol. Brain Res.*, **94**, 119–130.
23. Fleming, A. and Copp, A.J. (1998) Embryonic folate metabolism and mouse neural tube defects. *Science*, **280**, 2107–2109.

24. Applegarth, D.A., Toone, J.R. and Lowry, R.B. (2000) Incidence of inborn errors of metabolism in British Columbia, 1969–1996. *Pediatrics*, **105**, e10.
25. Nyhan, W.L. (1989) Nonketotic hyperglycinemia. In Scriver, C.R., Beaudet, A.L., Sly, W.S. and Valle, D. (eds), *The Metabolic Basis of Inherited Disease*. McGraw-Hill, Inc., New York, 743–753.
26. Kure, S., Kato, K., Dinopoulos, A., Gail, C., DeGrauw, T.J., Christodoulou, J., Bzduch, V., Kalmanchey, R., Fekete, G., Trojovsky, A. *et al.* (2006) Comprehensive mutation analysis of GLDC, AMT, and GCSH in nonketotic hyperglycinemia. *Hum. Mutat.*, **27**, 343–352.
27. Harris, M.J. (2008) Insights into prevention of human neural tube defects by folic acid arising from consideration of mouse mutants. *Birth Defects Res. A Clin. Mol. Teratol.*, **85**, 331–339.
28. Watanabe, M., Osada, J., Aratani, Y., Kluckman, K., Reddick, R., Malinow, M.R. and Maeda, N. (1995) Mice deficient in cystathionine β-synthase: animal models for mild and severe homocyst(e)inemia. *Proc. Natl Acad. Sci. USA*, **92**, 1585–1589.
29. Champion, K.M., Cook, R.J., Tollaksen, S.L. and Giometti, C.S. (1994) Identification of a heritable deficiency of the folate-dependent enzyme 10-formyltetrahydrofolate dehydrogenase in mice. *Proc. Natl Acad. Sci. USA*, **91**, 11338–11342.
30. Chen, Z., Karaplis, A.C., Ackerman, S.L., Pogribny, I.P., Melnyk, S., Lussier-Cacan, S., Chen, M.F., Pai, A., John, S.W., Smith, R.S. *et al.* (2001) Mice deficient in methylenetetrahydrofolate reductase exhibit hyperhomocysteinemia and decreased methylation capacity, with neuropathology and aortic lipid deposition. *Hum. Mol. Genet.*, **10**, 433–443.
31. MacFarlane, A.J., Liu, X., Perry, C.A., Flodby, P., Allen, R.H., Stabler, S.P. and Stover, P.J. (2008) Cytoplasmic serine hydroxymethyltransferase regulates the metabolic partitioning of methylenetetrahydrofolate but is not essential in mice. *J. Biol. Chem.*, **283**, 25846–25853.
32. Di, P.E., Sirois, J., Tremblay, M.L. and Mackenzie, R.E. (2002) Mitochondrial NAD-dependent methylenetetrahydrofolate dehydrogenase-methenyltetrahydrofolate cyclohydrolase is essential for embryonic development. *Mol. Cell. Biol.*, **22**, 4158–4166.
33. Swanson, D.A., Liu, M.L., Baker, P.J., Garrett, L., Stitzel, M., Wu, J.M., Harris, M., Banerjee, R., Shane, B. and Brody, L.C. (2001) Targeted disruption of the methionine synthase gene in mice. *Mol. Cell. Biol.*, **21**, 1058–1065.
34. Elmore, C.L., Wu, X., Leclerc, D., Watson, E.D., Bottiglieri, T., Krupenko, N.I., Krupenko, S.A., Cross, J.C., Rozen, R., Gravel, R.A. and Matthews, R.G. (2007) Metabolic derangement of methionine and folate metabolism in mice deficient in methionine synthase reductase. *Mol. Genet. Metab.*, **91**, 85–97.
35. Field, M.S., Anderson, D.D. and Stover, P.J. Mthfs is an essential gene in mice and a component of the purinosome. *Front. Genet.* http://www.frontiersin.org/nutrigenomics/10.3389/fgene.2011.00036/abstract.
36. Spiegelstein, O., Mitchell, L.E., Merriweather, M.Y., Wicker, N.J., Zhang, Q., Lammer, E.J. and Finnell, R.H. (2004) Embryonic development of folate binding protein-1 (Folbp1) knockout mice: effects of the chemical form, dose, and timing of maternal folate supplementation. *Dev. Dyn.*, **231**, 221–231.
37. Burren, K.A., Savery, D., Massa, V., Kok, R.M., Scott, J.M., Blom, H.J., Copp, A.J. and Greene, N.D.E. (2008) Gene-environment interactions in the causation of neural tube defects: folate deficiency increases susceptibility conferred by loss of *Pax3* function. *Hum. Mol. Genet.*, **17**, 3675–3685.
38. Beaudin, A.E., Abarinov, E.V., Noden, D.M., Perry, C.A., Chu, S., Stabler, S.P., Allen, R.H. and Stover, P.J. (2011) Shmt1 and de novo thymidylate biosynthesis underlie folate-responsive neural tube defects in mice. *Am. J. Clin. Nutr.*, **93**, 789–798.
39. Nijhout, H.F., Reed, M.C., Lam, S.L., Shane, B., Gregory, J.F. III and Ulrich, C.M. (2006) In silico experimentation with a model of hepatic mitochondrial folate metabolism. *Theor. Biol. Med. Model.*, **3**, 40.
40. Pike, S.T., Rajendra, R., Artzt, K. and Appling, D.R. (2010) Mitochondrial C1-tetrahydrofolate synthase (MTHFD1L) supports the flow of mitochondrial one-carbon units into the methyl cycle in embryos. *J. Biol. Chem.*, **285**, 4612–4620.
41. Dunlevy, L.P.E., Burren, K.A., Mills, K., Chitty, L.S., Copp, A.J. and Greene, N.D.E. (2006) Integrity of the methylation cycle is essential for mammalian neural tube closure. *Birth Defects Res. A*, **76**, 544–552.
42. Greene, N.D., Stanier, P. and Moore, G.E. (2011) The emerging role of epigenetic mechanisms in the aetiology of neural tube defects. *Epigenetics*, **6**, 875–893.
43. Apostolidou, S., Abu-Amero, S., O'Donoghue, K., Frost, J., Olafsdottir, O., Chavele, K.M., Whittaker, J.C., Loughna, P., Stanier, P. and Moore, G.E. (2007) Elevated placental expression of the imprinted PHLDA2 gene is associated with low birth weight. *J. Mol. Med.*, **85**, 379–387.
44. Niwa, H., Yamamura, K. and Miyazaki, J. (1991) Efficient selection for high-expression transfectants with a novel eukaryotic vector. *Gene*, **108**, 193–199.
45. Oda, M., Kure, S., Sugawara, T., Yamaguchi, S., Kojima, K., Shinka, T., Sato, K., Narisawa, A., Aoki, Y., Matsubara, Y. *et al.* (2007) Direct correlation between ischemic injury and extracellular glycine concentration in mice with genetically altered activities of the glycine cleavage multienzyme system. *Stroke*, **38**, 2157–2164.
46. Fujiwara, K., Okamura-Ikeda, K. and Motokawa, Y. (1991) Lipoylation of H-protein of the glycine cleavage system. The effect of site-directed mutagenesis of amino acid residues around the lipoyllysine residue on the lipoate attachment. *FEBS Lett.*, **293**, 115–118.
47. Wlodarczyk, B.J., Tang, L.S., Triplett, A., Aleman, F. and Finnell, R.H. (2006) Spontaneous neural tube defects in splotch mice supplemented with selected micronutrients. *Toxicol. Appl. Pharmacol.*, **213**, 55–63.
48. Essien, F.B. and Wannberg, S.L. (1993) Methionine but not folinic acid or vitamin B-12 alters the frequency of neural tube defects in *Axd* mutant mice. *J. Nutr.*, **123**, 27–34.
49. Nakai, T., Nakagawa, N., Maoka, N., Masui, R., Kuramitsu, S. and Kamiya, N. (2005) Structure of P-protein of the glycine cleavage system: implications for nonketotic hyperglycinemia. *EMBO J.*, **24**, 1523–1536.

Seizure 21 (2012) 55–60

Contents lists available at ScienceDirect

Seizure

journal homepage: www.elsevier.com/locate/yseiz

Case report

Epilepsy in RAS/MAPK syndrome: Two cases of cardio-facio-cutaneous syndrome with epileptic encephalopathy and a literature review

Masao Adachi [a,*], Yu Abe [b], Yoko Aoki [b], Yoichi Matsubara [b]

[a] Department of Pediatrics, Kakogawa Hospital Organization, Kakogawa West-City Hospital, 384-1 Hiratsu, Yoneda-cho, Kakogawa, Hyogo 675-8611, Japan
[b] Department of Medical Genetics, Tohoku University School of Medicine, Sendai, Japan

ARTICLE INFO

Article history:
Received 30 May 2011
Accepted 29 July 2011

Keywords:
Cardio-facio-cutaneous syndrome
RAS/MAPK pathway
Neurological impairment
Seizure

ABSTRACT

We report two individual cases of cardio-facio-cutaneous (CFC) syndrome with severe neurological impairment consisting of infantile spasms with hypsarrhythmia and refractory epilepsy with multifocal epileptic paroxysms such as modified hypsarrhythmia. Both cases shared diffuse brain atrophy and severely delayed myelination on neuroimaging. Genetic analysis revealed individual heterozygous mutations in the KRAS (phenotype of CFC/Noonan syndrome) and BRAF genes (phenotype of CFC syndrome). Neurological impairment in cases with mutations in the RAS/MAPK (mitogen activated protein kinase) signal pathway may be more severe, and could be linked to some forms of refractory epilepsy, especially epileptic encephalopathy that includes infantile spasms.

1. Introduction

Cardio-facio-cutaneous (CFC) syndrome is a very rare and sporadic disease that includes the characteristics of dysmorphic facial appearance, ectodermal abnormalities, cardiac abnormalities, growth retardation and neuro-developmental delay. This syndrome is categorized as one of the RAS/MAPK syndromes, which cause altered signal transduction of the RAS/MAPK (mitogen activated protein kinase) pathway, including BRAF, MEK1/2, and KRAS.[1–3] Compared with other RAS/MAPK syndromes, such as Costello syndrome and Noonan syndrome, CFC syndrome exhibits a more severe phenotype including severe neurological impairment, seizures, and developmental delay. We describe the clinical details of neurological findings in two cases of genetically determined CFC syndrome which displayed refractory epilepsies diagnosed as infantile spasms and other epileptic encephalopathy, and we then compare our results with those of similar literature findings.

2. Case reports

2.1. Case 1: six-year-old boy

A large-for-date boy was delivered as the first child to healthy and non-consanguineous Japanese parents (mother 42 years old and father 31 years old) at 32 weeks of gestational age with a birth weight of 3758 g and with moderate neonatal asphyxia (an Apgar score of 6 at 5 min after birth) following a normal pregnancy. The patient was intensively treated in the neonatal intensive care unit (NICU) in our hospital. Postnatal screening showed fetal hydrops with heart failure due to severe pulmonary valve stenosis which was treated with diuretics and beta blockers. Peculiar craniofacial features included "coarse face," curly hair, prominent forehead, downslanting palpebral fissures, short nose and broad nasal tip with anteverted nares, low-set dysmorphic and posteriorly angulated ears, abnormal skin (loose and pigmented skin with deep furrows and multiple lentigo, wrinkled palms with deep palmar and plantar creases), webbed neck, chest deformity, and micromelic dwarfism (Fig. 1A).

At three days postnatal, myoclonic seizures of the extremities occurred which were controlled by administration of bolus midazolam (MDL). At the age of 11 months, he developed repetitive series-formed tonic spasms, and the interictal electroencephalogram (EEG) showed hypsarrhythmia (Fig. 1C). Valproic acid (VPA), clonazepam (CZP), and zonisamide (ZNS) were ineffective in reducing seizure frequency and improving EEG findings, and complete remission was only obtained by one course of low dose (0.025 mg/kg) adrenocorticotropic hormone (ACTH). Since undergoing ACTH therapy, he has had no episodes of epileptic seizures while undergoing VPA monotherapy until the present age of six years, but his most recent (interictal) EEG showed asynchronous, high-voltage slow waves with irregular spike-waves, or polyspikes with/without waves dominantly in the right temporal-occipital region (Fig. 1D). Magnetic resonance imaging (MRI) at three years of age revealed agenesis of the corpus callosum, ventricular dilatation, diffuse cortical atrophy and severely delayed myelination (Fig. 1B). Tracheotomy was performed and persistent mechanical ventilation

* Corresponding author. Tel.: +81 79 432 3531; fax: +81 79 432 3672.
E-mail address: ama-p@rc4.so-net.ne.jp (M. Adachi).

1059-1311/$ – see front matter © 2011 British Epilepsy Association. Published by Elsevier Ltd. All rights reserved.
doi:10.1016/j.seizure.2011.07.013